AMERICAN UNIVERSITY OF BEIRUT

UNVEILING THE NEURAL NETWORK UNDERLYING THE GENERATION OF NEURAL SEQUENCES IN THE HVC THROUGH COMPUTATIONAL MODELING

by
MARC JEAN CHAMMAS

A thesis
submitted in partial fulfillment of the requirements
for the degree of Master of Science
to the Biomedical Engineering Program
of the Maroun Semaan Faculty of Engineering and Architecture
at the American University of Beirut

Beirut, Lebanon
September 2020

AMERICAN UNIVERSITY OF BEIRUT

UNVEILING THE NEURAL NETWORK UNDERLYING THE GENERATION OF NEURAL SEQUENCES IN THE HVC THROUGH COMPUTATIONAL MODELING

by

MARC JEAN CHAMMAS

Approved by: [Signature]

_____Arij Daou_____

[Dr. Arij Daou, Assistant Professor] Advisor
[Biomedical Engineering Program]
Maroun Semaan Faculty of Engineering and Architecture

[Signature]

_____Noel Ghanem_____

[Dr. Noel Ghanem, Associate Professor] Co-advisor
[Department of Biology]
Faculty of Arts and Sciences

[Signature]

_____ _____

[Dr. Massoud Khraiche, Assistant Professor] Member of Committee
[Biomedical Engineering Program]
Maroun Semaan Faculty of Engineering and Architecture

[Signature]

_____ _____

[Dr. Fadi Karameh, Associate Professor] Member of Committee
[Department of Electrical and Computer Engineering]
Maroun Semaan Faculty of Engineering and Architecture

Date of thesis/dissertation defense: September 8, 2020

AMERICAN UNIVERSITY OF BEIRUT

THESIS, DISSERTATION, PROJECT RELEASE FORM

Chammas	Marc	
Last	First	Middle

● Master's Thesis ○ Master's Project ○ Doctoral Dissertation

[X] I authorize the American University of Beirut to: (a) reproduce hard or electronic copies of my thesis, dissertation, or project; (b) include such copies in the archives and digital repositories of the University; and (c) make freely available such copies to third parties for research or educational purposes.

[ ] I authorize the American University of Beirut, to: (a) reproduce hard or electronic copies of it; (b) include such copies in the archives and digital repositories of the University; and (c) make freely available such copies to third parties for research or educational purposes

After: **One ---- year from the date of submission of my thesis, dissertation, or project.**
Two ---- years from the date of submission of my thesis, dissertation, or project.
Three ---- years from the date of submission of my thesis, dissertation, or project.

September 11, 2020

Signature Date

This form is signed when submitting the thesis, dissertation, or project to the University Libraries

ACKNOWLEDGMENTS

I would like to start by thanking my thesis advisor Dr. Arij Daou for his continuous support throughout my graduate studies. I had the honor to work with him on my thesis project and I highly appreciate his professionalism along with his values and morals.

I would also like to thank my thesis committee members: Dr. Noel Ghanem, Dr. Massoud Khraiche and Dr. Fadi Karameh for their insightful and constructive comments.

Finally, I am sincerely grateful to my parents whose love and support always motivate me to get to the better version of me. I am thankful for their care and reassurance that always helped me in overcoming obstacles and hard times I have been through throughout life. This accomplishment would not have been possible without them.

AN ABSTRACT OF THE THESIS OF

Marc Chammas for Master of Science
Major: Biomedical Engineering

Title: Unveiling the neural network underlying the generation of neural sequences in the HVC through computational modeling

Birdsong offers a unique model system to understand how a developing brain – once given a set of purely acoustic targets – teaches itself the vocal-tract gestures necessary to imitate those sounds. Like human infants, juvenile male zebra finches (Taeniopygia guttata) passes through the stages of learning the vocal-motor gestures of adult sounds.

The HVC nucleus (avian brain region, used as a proper name) is a cortical nucleus in the forebrain that is responsible for the songbird's singing as well as the learning process of his song. The HVC consists of three neural populations: basal-ganglia-projecting (HVC_X) neurons, forebrain-projecting (HVC_{RA}) neurons and interneurons (HVC_{INT}). Each neuron population has its own cellular, electrophysiological and functional properties. In particular, HVC_{RA} neurons emit a single 6-10 ms burst of action potentials at the same exact time during each rendition of song, HVC_X neurons fire 1 to 3 bursts that are also time locked to vocalizations, while HVC_{INT} neurons fire and burst randomly with high firing frequency throughout song with no significant pattern. As a population, these three classes of HVC neurons form an explicit representation of time and are responsible for orchestrating song learning and production; yet little is known about their functional connectivity within nucleus HVC and how they work cooperatively to control learning and singing.

Very few mathematical models have been developed to describe HVC's neural activity, and all of the generated models were either non-biological plausible or replicating *in vitro* data collected from brain slices. We developed a conductance-based Hodgkin Huxley model for the three classes of HVC neurons and connected them in several networks via different architecture patterning scenarios with the aim to replicate the *in vivo* firing patterning behaviors. We are able throughout these networks to reproduce the *in vivo* behavior of these neurons as shown by the experimental recordings. The study of the synaptic architecture of the HVC nucleus has given us insights on the nature of the physiological changes taking place inside the bird's brain during learning and vocalization providing a large step towards biologically plausible descriptions of the underlying *in vivo* neural networks.

CONTENTS

LIST OF ILLUSTRATIONS

connections had been reported between HVC_{RA} and HVC_X (dashed arrow).

6 Spike raster plot of ten HVC_{RA} neurons and two HVC interneurons recorded in one bird during singing (left) and call vocalizations (right). Each row of tick marks shows spikes generated during one rendition of the song or call; roughly ten renditions are shown for each neuron. Neural activity is aligned by the acoustic onset of the nearest syllable. HVC_{RA} neurons burst reliably at a single precise time in the song or call; however, HVC interneurons spike or burst densely throughout the vocalizations (Hahnloser et al., 2003). 33

7 Mathematical model simulations of HVC neurons. A: HVC_X model neuron parameters were calibrated to match the voltage traces of a depolarizing pulse of 100 pA. B: Model HVC_X neuron exhibiting a weak sag in response to negative current pulses (compare Fig. 7A-B to Fig. 7A-B). C: HVC_{RA} model neuron parameters were calibrated to match the experimental recording (I_{app} = 150 pA). The long delay to spiking is due to the A-type K current (I_A). D: For the same parameter values used in C, the HVC_{RA} model neuron has no sag but exhibits inward rectification in the spacing between voltage traces (compare Fig. 7C-D to Fig. 7C-D). E: HVC_{INT} model neuron exhibiting high firing frequency with no adaptation in response to 75 pA current pulse. F: The same model HVC_{INT} neuron exhibiting prominent sag and strong rebound burst in response to negative current pulses (compare Fig. 7E-F to Fig. 7E-F). 37

8 Model output compared to experimental results obtained by Mooney et al. 2005 (Mooney & Prather, 2005). A1: HVC_{RA} to HVC_X connectivity as seen in experimental recordings. A2: HVC_{RA} to HVC_X model connectivity; a depolarizing current of 500 pA was applied to HVC_{RA} for 500 ms. B1: HVC_{RA} to HVC_{INT} connectivity as seen in experimental recordings.B2: HVC_{RA} to HVC_{INT} model connectivity. A depolarizing current of 200 pA was applied to HVC_{RA} for 500 ms. 48

9 Model output compared to experimental results obtained by Mooney et al. 2005 (Mooney & Prather, 2005). A1: HVC_{INT} to HVC_X connectivity as seen in experimental recordings. A2: HVC_{INT} to HVC_X model connectivity; a depolarizing current of 200 pA was applied to HVC_{INT}. B1: HVC_{INT} to HVC_X connectivity as seen in experimental recordings. B2: HVC_X to HVC_{INT} model connectivity. A depolarizing current of 200pA was applied to HVC_{INT} for 500 ms. C1: HVC_X to HVC_{INT} connectivity as seen in experimental 49

recordings. C2: HVC_X to HVC_{INT} model connectivity. A depolarizing current of 1000 pA was applied to HVC_X.

10 Network 1 design structure. Black arrows symbolize excitation via AMPA currents. The red arrow onto HVC_{RA}^{1} represents the excitatory drive (DC current) from outside the HVC. 51

11 HVC_{RA} spiking patterns of network architecture one. Sequential bursting of 40 different HVC_{RA} neurons (labeled with numbers) showing the propagation of sequential activity independent of HVC_X and HVC_{INT} neurons. The neural traces are aligned by the acoustic elements of a spectrogram from a bird's song illustrating the firing of HVC_{RA} neurons with respect to ongoing song. 53

12 Firing patterns of two sample HVC_{RA} neurons (HVC_{RA}^{2} and HVC_{RA}^{3}) in the chain. The duration between the burst of one HVC_{RA} neuron and the burst in the next HVC_{RA} neuron in the chain is ~ 5 ms. This duration of time is solely dependent on the strength of the synaptic conductance that connects the two neurons in the chain. 54

13 Arrangement of prototype network architecture two. Two classes of HVC_{INT} neurons are presented (HVC_{INTA} in red and HVC_{INTB} in grey). Black arrows symbolize excitation via AMPA currents. Red arrows (with circle heads) symbolize inhibition via GABA currents. Blue arrows symbolize excitatory drive (DC inputs) from outside the HVC. The first microcircuit is enclosed by a dashed rectangle to represent its role as a leading microcircuit in the network. 56

14 HVC spiking patterns of network architecture two. Class A and class B HVC interneurons firing pattern shown in panels A and B respectively. Class B interneurons fire continuously except at particular instances of time when they are inhibited by Class A interneurons. C: Sequential bursting of HVC_{RA} neurons within the network. 59

15 Spike raster plot of HVC_{RA} neurons showing the time locked firing of neurons relative to vocalizations. Each row of tick marks shows spikes generated during one rendition of the song or call; roughly ten renditions are shown for each neuron. HVC_{RA} neurons burst at a single precise time during the song. 60

16 Zoomed version of HVC spiking patterns of network architecture two: The burst in HVC_{INTA} (red) inhibits HVC_{INTB} (black) which allows HVCRA (blue) to escape inhibit and fire a burst of activity. 61

17 Arrangement of prototype network architecture three. Black arrows symbolize excitation via AMPA currents. Red arrows (with circle heads) symbolize inhibition via GABA currents. The blue arrow 63

while quick starting the network with a random DC input applied to HVC_{RA}^{1} .A: HVC_{RA} neurons show a sequential propagation of bursts throughout the network. B: HVC_{INT} neurons fire sparsely throughout the song while exhibiting several bursts of activity. C: HVC_{X} neurons fire different number of bursts (1-3 bursts) similar to experimental results.

LIST OF TABLES

LIST OF ABBREVIATIONS

AFP : anterior forebrain pathway

BOS : bird's own song

C_m : membrane capacitance

DLM : medial dorsolateral nucleus of the thalamus

DM : dorsomedial part of the intercollicular nucleus in the midbrain

FHU : functional HVC unit

GPe : external globus pallidus

GPi : internal globus pallidus

g_A : A type potassium current conductance

g_{AMPA} : AMPA current conductance

g_{CaL} : high threshold L-type calcium current conductance

g_{CaT} : low threshold T-type calcium current conductance

$g_{GABA\text{-}A}$: GABA current conductance

g_h : hyperpolarization current conductance

g_K : potassium current conductance

g_{KNa} : sodium dependent potassium current conductance

g_L : leak current conductance

g_{Na} : sodium current conductance

g_{Nap} : persistent sodium current conductance

g_{NMDA} : NMDA current conductance

g_{SK} : small conductance calcium activated potassium current conductance

HVC : high vocal center

HVC_{INT} : HVC interneurons

HVC_{RA} : RA projecting neurons

HVC_X : X projecting neurons

I_A : A type potassium current

I_{AMPA} : AMPA synaptic current

I_{app} : applied current

I_{CaL} : high threshold L-type calcium current

I_{CaT} : low threshold T-type calcium current

$I_{GABA\text{-}A}$: GABA-A synaptic current

I_h : hyperpolarization current

I_K : potassium current

I_{KNa} : sodium dependent potassium current

I_L : leak current

I_{Na} : sodium current

I_{Nap} : persistent sodium current

I_{NMDA} : NMDA synaptic current

I_{SK} : small conductance calcium activated potassium current

LMAN : lateral portion of the magnocellular nucleus of the anterior neostriatum

nXIIts : tracheosyringeal division of the twelfth nucleus

NCM : caudomedial nidopallium

PAm : paraambigualis nucleus

PAG : periaqueductal gray

PPA : primary progressive aphasia

RA : robust nucleus of arcopallium

RAm : retroambigualis nucleus

Uva : uvaeform nucleus

VMP : vocal motor pathway

CHAPTER 1

INTRODUCTION

Complex behaviors are made possible due to the ability of the brain to move through well-defined sequences of neural states. Brain processes capable of generating propagating sequential activity are thought to underlie motor sequencing (Shima *et al.*, 2007), navigation (Mehta *et al.*, 2002; Harvey *et al.*, 2009), movement planning (Pastalkova *et al.*, 2008) and cognitive tasks (Georgopoulos *et al.*, 1989). Various brain regions have been associated with the control of temporal and ordinal structure of movement sequences (Lamendella, 1977; Bolhuis *et al.*, 2010; Highnam & Bleile, 2011; Price, 2012; Flinker *et al.*, 2015; Javed & Lui, 2019; Javed & Wroten, 2019). However, the underlying biophysical mechanisms through which neural circuits generate these sequences are very poorly understood.

Complex learned behaviors need prior planning of individual movement elements into a proper spatial and temporal ordered sequence. This premotor planning is necessary for events anticipation, movement selection and an exact actions order. For instance, speech is a result of complex neural network connectivity that requires various processes, starting from putting thoughts into words, then arranging words in a comprehensible structure, and finally coordinating the activity of the muscles responsible for the physical generation of speech which are normally uttered in a sequential manner that is governed by the laws of grammar and syntax.

Songbirds have emerged as an excellent model system for investigating the neural mechanisms of sequence generation because songbirds learn to sequence their song elements, analogous, in many ways, to how humans learn to produce spoken sequences with syntactic structure. Thus, determining how spoken language evolved is more likely to become clearer with concerted efforts in researching songbirds. Our overall aim is to understand the neural mechanisms of sequence generation through vocal production and learning by providing a quantitative description of the physiological variables that control vocal performance in a particular species of songbirds, the zebra finch (Fig. 1).

Figure 1: An adult male zebra finch

We will start by summarizing the anatomical and physiological identifications of speech and language acquisition in the mammalian brain and then continue to list the analogies between speech and birdsong and describe why birdsong is an attractive and important model to study not only language acquisition and production but also other backbone topics in neuroscience like learning, memory, neural sequence generation and many more along with their pathologies.

1.1. Speech and language processing in the human brain

Human speech is primarily controlled by the largest part of the brain known as the cerebrum (Fig. 2). In recent years, language processing in the brain has been at the core of attention of research studies (Lieberman, 2009; Highnam & Bleile, 2011; Price, 2012). As of today, it has been accepted that the control of speech is a result of complex network connectivity in the brain. Speech formation requires various processes, starting from putting thoughts into words, then arranging words in a comprehensible structure, and finally moving the tongue and the mouth along with respiratory control to generate correct sentences that abide by the laws of grammar and syntax.

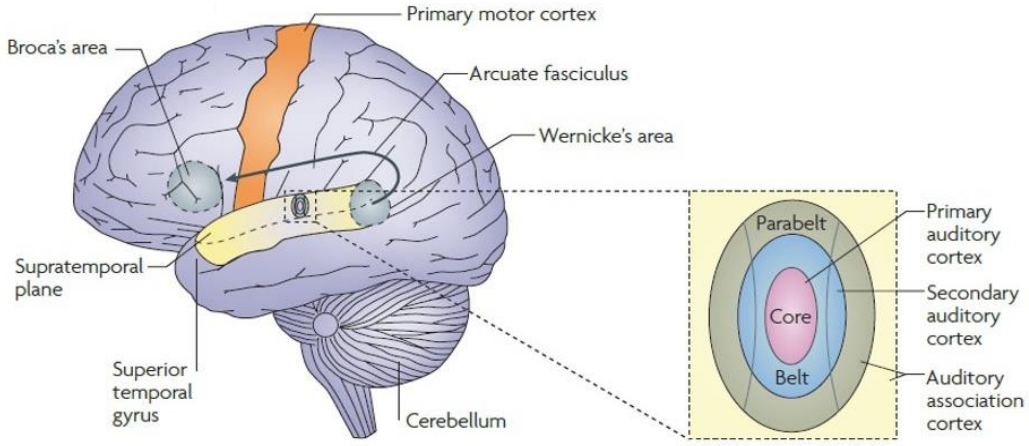

Figure 2: Schematic view of the left side of the human brain, showing regions that are involved in speech and language. Broca's area is particularly involved in speech production, whereas Wernicke's area is involved in speech perception and recognition. The two regions are connected by the arcuate fasciculus (Bolhuis et al., 2010).

Several areas of the brain interact cooperatively to control speech: the cerebrum, Broca's area, Wernicke's area, the arcuate fasciculus, the cerebellum, the motor cortex and elements of limbic system such as the cingulate cortex, the basal ganglia and the thalamus (Fig. 2). The frontal and the temporal lobes of the cerebrum, are primarily involved in speech formation and comprehension. Broca's area is located in the left frontal lobe of the brain and has an important role in turning thoughts into spoken words. This specialized area has been found to be most active right before we speak. Furthermore, Broca's area helps in passing information to the motor cortex, which controls the movements of the lips and the tongue (Price, 2012; Flinker *et al.*, 2015). Another essential area involved in speech control is the Wernicke's area. This area is mainly involved in the understanding and processing of speech and written language. Wernicke's area is located in the temporal lobe, just behind the ears (Price, 2012; Javed & Wroten, 2019). In fact, the temporal lobe is where sound is processed. Moreover, the arcuate fasciculus is a bundle of nerves connecting Wernicke's area to Broca's area that helps in forming words, speaking clearly and understanding concepts in language form. The cerebellum, located at the lower back of the brain, is involved in coordinating voluntary muscle movements like opening and closing the mouth, moving the limbs, and maintaining balance and a straight posture. The cerebrum controls language processing as well. To be able to speak clearly, we must move the muscles of the mouth, the tongue, and the throat adequately (Highnam & Bleile, 2011; Javed & Lui, 2019) which is made possible by the motor cortex. Located in the frontal lobe, the motor cortex receives input information from Broca's area and orders the muscles of the face, the mouth, the tongue, the lips, and the throat to move harmoniously to produce speech (Price, 2012; Javed & Lui, 2019).

The limbic system plays a key role in the speech control circuitry. This system combines primitive emotions and higher mental functions such as learning and memories formation. In terms of speech and language, the thalamus, the basal ganglia and the cingulate gyrus plays the most significant roles. The thalamus consists of nuclei that relay sensory inputs (i.e. auditory inputs) to other cortical areas. It entails as well higher order nuclei that propagate information from one cortical area to another. The thalamus main functions are the control of cortices connectivity and the filtering and routing of exchanged information. In terms of speech and language, this primarily refers to an exchange of lexical and semantic information during language perception and production (Klostermann, 2013). The cingulate gyrus has connections with speech and vocalization areas in the frontal lobes including Broca's area, which controls motor functions involved with speech production. Finally, the basal ganglia is a group of nuclei in the frontal lobe known to organize motor behavior and control, but mounting evidence suggests that this structure is involved in more cognitive domains such as language processing (Booth *et al.*, 2007), and complements the cortico-thalamic language processing mechanisms. Interestingly, the basal ganglia serves as a gating mechanism for physical movements, inhibiting potential movements until they are fully appropriate for the circumstances in which they are to be executed. This important structure plays a role in coordinating the release of the language plan, provided by the cortico-thalamic connectivity, into speech. In a nutshell, the basal ganglia plays a role in motor planning, working memory and words sequencing into comprehensible sentences. (Lamendella, 1977; Highnam & Bleile, 2011; Klostermann, 2013).

Moreover, lesions, traumas or infections occurring within the speech control loop are associated with several severe disabilities such as aphasias and apraxias. Aphasia is a condition associated with speaking or speech understanding problems, whereas apraxia is associated with troubles in putting together the correct muscle movements necessary to produce speech. Both abnormalities are mostly caused by a stroke or trauma to the brain. Symptoms of aphasia and apraxia depend on the damage location and its severity. When Broca's area is affected, the patient might find difficulties producing the sounds or may speak slowly or slur his words (Trost & Canter, 1974; Fridriksson *et al.,* 2015). The person can only produce short sentences limited to a maximum of four words. In this case, the patient suffers from Broca's aphasia or non-fluent aphasia. These symptoms may also appear in case of stroke or injuries damaging the areas of the brain responsible for controlling movements of the muscles of the mouth or the tongue. Damage to Wernicke's area may cause the patient to make up nonsense words or speak in meaningless long sentences. In this case, the patient suffers from Wernicke's aphasia or fluent aphasia. If the arcuate fasciculus is damaged, the patient shows inability repeating words he just heard; this happens in the case of conduction aphasia. Global aphasia might happen in case of widespread damage to the brain's language centers. People with this condition have difficulties expressing and understanding language (Trost & Canter, 1974; Obler *et al.*, 1978; Helasvuo *et al.,* 2001; Fridriksson *et al.,* 2015). In case of Alzheimer's disease, one of the most prevalent neurodegenerative diseases, the patient experiences gradual loss of speech over time. This is called primary progressive aphasia (PPA). This type of aphasia is a possible symptom of Alzheimer's disease while it can be an isolated disorder independently of Alzheimer's disease. Some people with primary progressive aphasia have

normal memories and are able to continue leisure activities or work. Primary progressive aphasia results from slow deterioration of areas of the brain used in speech in contrary to aphasia resulting from stroke or brain trauma which consequences appear right after the damage occurrence (Marczinski & Kertesz, 2006; Ahmed *et al.*, 2012). Usually, in case of aphasia or apraxia, speech-language therapy is prescribed. Whereas restoring full speech abilities following brain damage seem to be impossible, improvements could take place (Bragoni *et al.*, 2000; Stark & Warburton, 2018).

Collectively, this shows that speech generation and learning in the brain is a very complex mechanism that involves the coordination and control of various brain regions that works cooperatively to generate the sequential propagation of syllables and sounds. Pathologies in any of the associated areas of speech cause devastating effects on humans. Despite its importance, we know very little of the neurobiological underpinnings that control its underlying processes. While studying the speech circuitry in humans is more efficient in investigating these kind of pathologies, researching songbirds, that show remarkable similarities to humans in vocal learning and production, is still the most ethical and efficient way to investigate this circuitry.

1.2. The song learning process in songbirds

Both songbirds and humans learn vocalization at early stages of life. Vocal learning takes place in similar critical periods with a greater ability to learn during earlier life stages. Learning abilities may be decreased by biological factors or by the learning process itself

(Doupe & Kuhl, 1999). Human speech and bird songs learning show a strong dependence on hearing. To be able to learn and sing their song normally, birds should be able to hear their tutors as well as their own vocalizations via auditory feedback (Doupe & Kuhl, 1999). Similarly in humans, infants need to hear their parents speaking to learn how to speak. Deafening in either species have devastating effects on vocal learning and production. Not to mention that a delay in the auditory feedback, both in humans and songbirds, deteriorates the structure of the learned song (in adults) and prohibits its correct learning (in babies). This underlines the presence of similarities in the auditory pathways between these two species while emphasizing the important role of auditory feedback in maintaining vocalization throughout life (Doupe & Kuhl, 1999).

Neither songbirds nor babies appear to learn their communicative signals well except at specific periods in their lives. Human infants learn to produce vocalizations rapidly in a process that appears to be simple. A few months after birth, children begin to babble and at 3-4 years of age they can produce meaningful sentences with the correct syntax. This developmental path is exactly the same regardless of language type or culture. It had been a mystery for linguists, psychologists and neuroscientists to explain how children do this. Songbirds pass through developmental paths in song learning that are extremely similar to the paths that humans pass through during language acquisition (Thorpe, 1958). Vocal imitation starts from the babbling stage (in humans) or the sub-song stage (in songbirds) which then evolves to the complete complex communication system.

The song learning process entails several stages. In order to learn to sing, juvenile songbirds need to listen to and memorize the song of their father or a neighboring adult male conspecific or even from taped renditions of song. This is called the **sensory learning**

phase. Songbirds then conduct solo rehearsals of their own song using auditory feedback to match it to the memorized template. This is referred to as the **sensorimotor learning phase.** In zebra finches, as in many other species of songbirds, song learning can be divided into three stages: sub-song, plastic song and crystallized song. At the beginning birds produce a sub-song (earliest stage of singing). With practice, the sub-song evolves to a more structured song called plastic song. In this stage, the acoustic elements start to resemble those in the tutor song, but are still produced in a sequence that is variable (Margoliash & Schmidt, 2010). Finally, the song becomes crystallized where the young bird begins to produce a normal adult song exhibiting striking resemblance to the tutor song (Fee & Scharff, 2010). The adult songbird song is constituted of a repeated sequence of sounds, called a motif. Each motif, lasting for about a second, is composed of shorter bursts of sound called syllables (Fee & Scharff, 2010). Song learning phases have a different timing among songbirds. Zebra finches and white-crowned sparrows learn only during their first year of age; these birds are classified as age-limited learners. On the other hand, the canary and the European starling birds are open-ended learners; their song can be developed beyond the first year generally in a seasonal manner (Brenowitz *et al.*, 1997).

1.3. Avian song system anatomy

Songbirds have specialized, spatially distributed, compact and discrete brain nuclei that are interconnected through a series of pathways known as the “song system”. Very few of the neural circuits that are known to control behavior are anatomically as distinct as the song system (Brainard & Doupe, 2000) (Fig. 3).

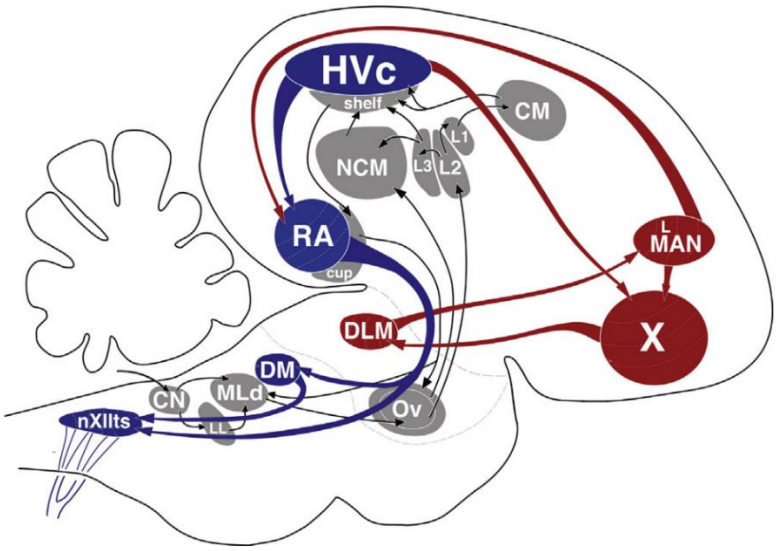

Figure 3: Sagittal perspective schematic of an adult male zebra finch brain shows the position of HVC in the dorsocaudal nidopallium. The vocal motor pathway (shown in blue) controls the vocal organ, or syrinx. Lesioning this pathway in adult or in juvenile males have devastating effects on song. The anterior forebrain pathway (shown in red) controls song learning. Lesions to nuclei within this loop affect song development but not the production of adult song. DLM, medial dorsolateral nucleus of the thalamus; LMAN, lateral portion of the magnocellular nucleus of the anterior neostriatum; nXIIts, the tracheosyringeal division of the twelfth nucleus; RA, robust nucleus of arcopallium (Daou et al., 2013).

Two major pathways are involved in song learning and song production: the descending vocal motor pathway (VMP) and the anterior forebrain pathway (AFP). The vocal motor pathway participates in song learning and controls song production. It includes the HVC nucleus, the robust nucleus of the arcopallium (RA) and the brain stem motor nucleus (Kozhevnikov & Fee, 2007). This pathway consists of projections from the thalamic nucleus and the neostriatal nucleus to the HVC. The HVC projects to the robust nucleus of the archistriatum (RA) providing it with premotor input. The RA at its turn projects to both the dorsomedial part of the intercollicular nucleus in the midbrain and to the tracheosyringeal part of the hypoglossal motor nucleus in the brain stem (nXIIts) that

innervates the bird's syrinx. The nXIIts nerve controls the muscles responsible for generating the vocal output. HVC_{RA} and RA neurons activity are in synchrony with song production in the syrinx. The RA projects to nuclei retroambigualis (RAm) and paraambigualis (PAm) that control the processes of respiration during singing. The AFP is a cortical basal ganglia loop; it includes a basal ganglia analogue known as the area X and the dorsolateral thalamic nucleus (DLM). The AFP plays a crucial role in song learning and recognition. The HVC projects to area X (basal ganglia) then to the medial nucleus of the DLM in the thalamus. Area X is responsible for song learning, recognition of the bird's own song (BOS), and for the song syllable sequencing. Nucleus DLM in its turn projects to the magnocellular nucleus of the anterior neostriatum (LMAN). Then, LMAN nucleus projects to area X and to the RA nucleus providing it with auditory input. Nucleus LMAN is considered as the output nucleus of the AFP. Projection neurons from LMAN to the RA nucleus gives the RA nucleus its essential role in maintaining the song structure and correcting potential errors through auditory feedback. Thus, the RA nucleus receives glutamatergic synaptic projections from both the HVC and LMAN nuclei. Finally, the HVC nucleus receives afferents from the uvaeform (Uva) nucleus located in the thalamus (Brenowitz *et al.,* 1997; Fee & Scharff, 2010).

1.4. Vocal production analogy: humans and songbirds

Regions of the songbird brain involved in vocal production and auditory perception are analogous, in many ways, to the human brain regions involved in producing and learning speech. The caudomedial nidopallium (NCM) of songbirds is thought to be the avian equivalent of the human auditory association cortex in the temporal lobe, including

Wernicke's area (Bolhuis *et al.*, 2010). In addition to its role in auditory perception, the NCM is involved as well in auditory memory (Chew *et al.*, 1996). Nucleus HVC plays an important role in song production and sensorimotor learning (Hahnloser *et al.*, 2003; Day *et al.*, 2009), and it is thought to be the functional analogous to Broca's area located in the human frontal lobe (Doupe & Kuhl, 1999; Bolhuis & Gahr, 2006). Similarly vocal production and auditory recognition are controlled by different regions in the songbird brain (Gobes & Bolhuis, 2007). Moreover, nuclei NCM and HVC, in zebra finches, has been found to be subject to left brain lateralization similarly to human brain regions associated with speech and language (Moorman *et al.*, 2012).

Similarities are observed in behavioral deficits following lesions to brain areas involved in vocal learning in songbirds and humans. Left hemispheric lesions of nuclei HVC and RA in canaries cause similar deficits to those found after damage to human's left motor cortex; these lesions induce muteness for learned vocalizations or speech (Jürgens, 1995). Nucleus RA which is involved in learning, vocal motor control and song production in songbirds is the analogue of the motor and cingulate cortices in humans. Lesions to avian nXIIts and DM, just like lesions to the mammalian PAG, induce muteness in songbirds and humans respectively (Esposito *et al.*, 1999). Furthermore, lesions to songbird LMAN cause similar disabilities to those found after damage to anterior regions of the human premotor cortex, such as disruption of imitation or sequencing problems. Lesions to the songbird's LMAN nucleus just as lesions to the human insula and Broca's area induce poor imitation and syntax production difficulties. Similarly lesions to area X in songbirds just as lesions to the human anterior striatum result in disruption of vocal learning, poor imitation of sound (Kobayashi *et al.*, 2001), and syllable abnormalities(Lieberman, 2009). Moreover, area X in

songbirds is comprised of two pallidal like cell types: the thalamus projecting neurons innervated by the striatal like neurons (analog to the direct (GPi) pathway neurons of the mammalian basal ganglia) and locally projecting pallidal neurons (analog to the classical indirect (GPe) neurons). Based on observations, the singing-related firing patterns of these two cell classes are similar to those of neurons observed in the internal and external pallidal segments (GPi and GPe) in humans (Goldberg & Fee, 2010). Finally, similar to previous reports on the songbird's DLM nucleus (Halsema & Bottjer, 1991), damage to anterior parts of the human thalamus can lead to verbal aphasias (Graff-Radford *et al.*, 1985). Therefore, diseases of the cortical circuitry that underlie vocal learning and production have devastating motor and cognitive consequences, highlighting the importance of understanding the biophysical and circuit mechanisms that underlie the learning and generation of complex behaviors.

CHAPTER 2

LITERATURE REVIEW

Nucleus HVC plays a key role in the song system. It constitutes an essential pillar of the premotor pathway necessary for song production. Neurons in the HVC serve the role of the conductor of the song, having a pattern-generating role coding for syllable order and controlling the overall temporal structure of birdsong. The HVC serves as a primary source of input to the anterior forebrain pathway (AFP) essential in vocal learning. Due to its essential role, the HVC is one of the most studied structure in the song control system. Previous studies have suggested that the syllable order and tempo of the song are generated by HVC (Vu *et al.*, 1994), and that an HVC neural code for syllables is transformed into a code for shorter acoustic elements through the projection of HVC onto RA (Albert & Margoliash, 1996; Troyer & Doupe, 2000).

A very helpful way to decipher the HVC code and understand the neural mechanisms behind birds singing is to understand how HVC neurons respond *in vivo* during singing as well as *in vitro* when the neurons are stimulated with a patch pipette. We will be summarizing next the characteristic patterns of the three classes of HVC neurons.

2.1. Electrophysiological properties of HVC neurons *in vitro*

There are three different neuronal populations in HVC: neurons that project to area X (HVC_X) innervating a basal ganglia pathway necessary for vocal plasticity, neurons that

project to the RA (HVC_{RA}) innervating song premotor areas and interneurons (HVC_{INT}). Numerous *in vivo* and *in vitro* intracellular recording studies of HVC neurons have been carried out (Katz & Gurney, 1981; Kubota & Saito, 1991; Lewicki & Konishi, 1995; Lewicki, 1996; Dutar *et al.*, 1998; Kubota & Taniguchi, 1998; Schmidt & Perkel, 1998; Mooney, 2000; Mooney *et al.*, 2001; Mooney & Prather, 2005; Solis & Perkel, 2005; Wild *et al.*, 2005; Long *et al.*, 2010; Shea *et al.*, 2010; Daou *et al.*, 2013; Daou & Margoliash, 2020) . These studies shed light on several neuronal and circuit mechanisms and unveiled a variety of physiological properties within the HVC. For example, the brain slice studies demonstrated that HVC_{RA}, HVC_X, and HVC_{INT} neurons have distinct, categorical electrophysiological phenotypes (Kubota & Saito, 1991; Dutar *et al.*, 1998; Kubota & Taniguchi, 1998; Mooney, 2000; Mooney *et al.*, 2001; Mooney & Prather, 2005; Wild *et al.*, 2005; Shea *et al.*, 2010). The studies published this far have characterized HVC neurons according to their responses to depolarizing and hyperpolarizing current injections.

HVC_{RA}, HVC_X and HVC_{INT} neurons show different firing properties *in vitro*. In a nutshell, HVC_X neurons show a regular firing pattern with spike-frequency adaptation in response to depolarizing stimuli (Fig. 4A); when the neuron is depolarized with a relatively weak pulse, it starts firing at high frequency then promptly switches to a lower frequency that gradually decreases over time. This frequency adaptation had been shown pharmacologically that is due to I_{SK} and I_{KNa} (Daou *et al.*, 2013). In response to hyperpolarizing current pulses, HVC_X neurons show a fast and time-dependent inward rectification where a moderate sag appears in response to negative pulses (Fig. 4B). The sag is mainly due to the hyperpolarization activated inward current (I_h) while the rebound firing

is mainly due to the cooperation between $I_{CaT}$and I_h(Daou et al., 2013). Furthermore, HVC_X neurons are silent in the absence of synaptic currents.

HVC_{RA} neurons on the other hand are known for their relative lack of excitability in response to depolarizing current pulses (Daou *et al.*, 2013). Despite the increased magnitude of the depolarizing current pulses, the neuron usually fires one to several action potentials in response to the depolarizing pulse; this firing is usually accompanied by a long delay that's shown to be orchestrated by the A-type K^+ current (I_A) (Fig. 4C, (Daou *et al.*, 2013)). Also, HVC_{RA} generally have a much more negative hyperpolarized resting membrane potential compared to HVC_X neurons and interneurons (Fig. 4). Another key property of HVC_{RA} neurons is the absence of the sag and the rebound firing in response to hyperpolarizing current pulses (Fig. 4D). I_A had been shown to be the main player in damping the excitability of the HVC_{RA} neuron with the cooperation of I_{SK} and I_{KNa} (Daou *et al.*, 2013). The after-hyperpolarization current (I_{SK}) also contributes to maintaining the extremely negative resting membrane potential of these neurons. Some also suggested the presence of two physiologically distinct classes of HVC_{RA} neurons that could fire phasically or tonically in response to a depolarizing current (Shea *et al.*, 2010).

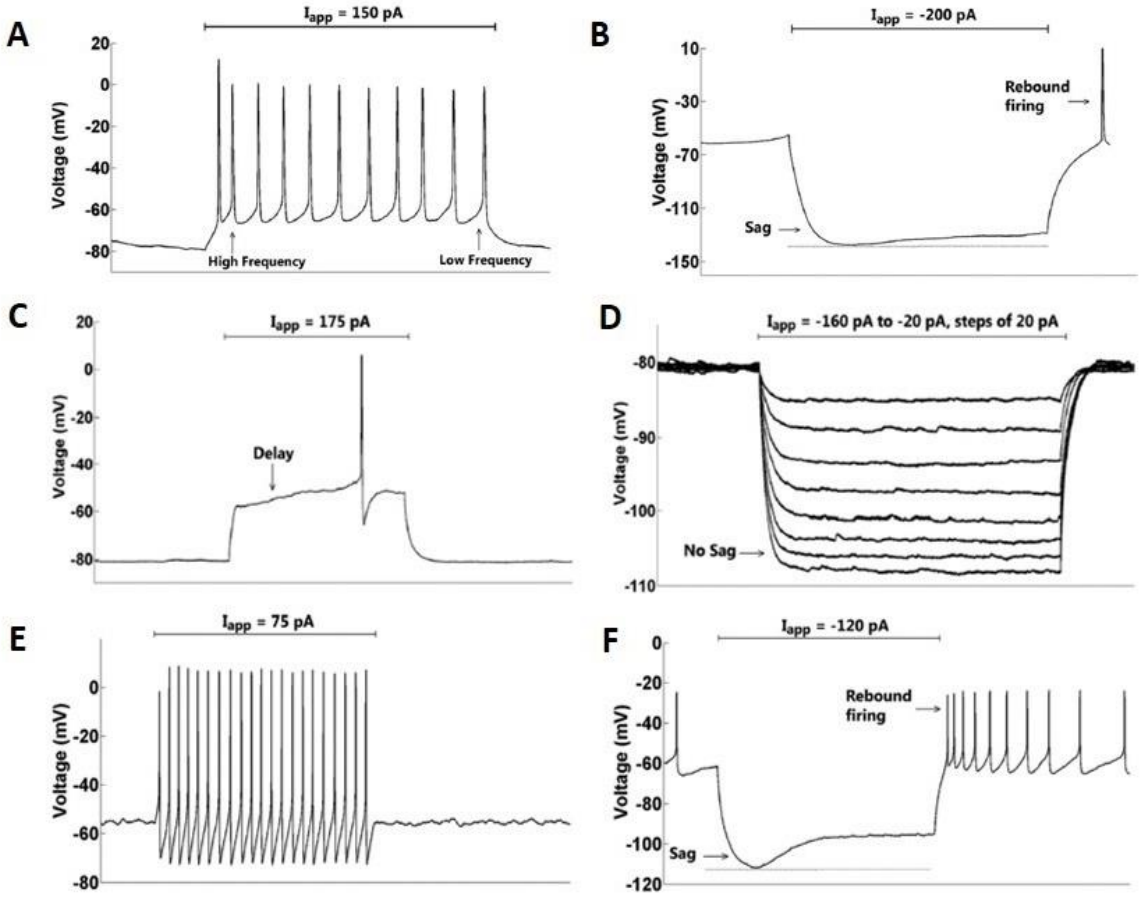

Figure 4: Firing properties of HVC neurons. A: A sample HVC_X neuron recorded in vitro exhibiting spike frequency adaptation in response to a depolarizing current pulse (150 pA). B: The same neuron exhibits a weak sag followed by post-inhibitory rebound firing in response to a hyperpolarizing current pulse (-200 pA). C: An HVC_{RA} neuron fires a single action potential, often with a long delay, in response to a relatively large depolarizing pulse (175 pA). D: The same HVC_{RA} neuron exhibits no sag in response to hyperpolarizing current pulses (-160 to -20 pA, in steps of 20 pA). E: An HVC interneuron fires tonically at high frequencies in response to a depolarizing current pulse (75 pA). F: The same HVC interneuron exhibiting a prominent sag followed by post-inhibitory rebound firing in response to a hyperpolarizing current pulse (-120 pA). Figures adopted from (Daou et al., 2013).

Finally, HVC interneurons are characterized by a high firing frequency in response to depolarizing currents (Fig. 4E). Interneurons exhibit tonic firing at a high frequency with almost no spike frequency adaptation (Daou *et al.*, 2013). Moreover they display a very prominent sag much greater than that of HVC_X neurons with a post-inhibitory rebound firing in response to hyperpolarizing current pulses (Fig. 4F). In general, HVC_{INT} neurons exhibit a resting membrane potential around -60mV while this potential falls around -72mV for HVC_X neurons and reaches its lowest value of -85mV for HVC_{RA} neurons.

Beside the classification of HVC neurons based on their ionic channels, HVC neurons have been stratified into four classes (I, IIa, IIb, III and IV) based on their different electrophysiological and morphological properties (Dutar *et al.*, 1998; Kubota & Taniguchi, 1998). Type I neurons were found to have large somata accompanied by spiny thick dendrites; most of them project to Area X. Type II neurons have been divided into two subclasses: neurons IIa have small somata and thin dendrites, while neurons IIb are characterized by their relatively large somata and thick dendrites. Type IIa neurons show similar electrical properties to HVC_{RA} neurons. Furthermore, type III neurons have beaded dendrite sand exhibit tonic firing with almost no adaptation, reminiscent of HVC interneurons. Finally, type IV neurons exhibit very small somata, as well as thin, short and spiny dendrites. Some of these neurons project to RA (Kubota & Taniguchi, 1998).

Various excitatory and inhibitory signals give rise to characteristic firing patterns in these neurons. Multiple lines of evidence indicates the presence of various classes of interneurons (Wild *et al.*, 2005), with interneurons showing distinct expressions of calcium binding-proteins (parvalbumin, caldinbin, calretinin). While we know that there are multiple classes of interneurons based on the staining protocols (Wild *et al.*, 2005), it

remains an open question to know to what extent there exists in reality three different classes of HVC interneurons that exhibit different electrophysiological properties as in other rat models (Gulyás *et al.*, 1996; Gritti *et al.*, 2003).

In their recently published paper, Daou and Margoliash (2020) showed that HVC_X neurons exhibit brief intense bursts of spikes during singing (Daou & Margoliash, 2020). Interestingly, HVC_X neurons spiking pattern for a specific bird showed similar onsets, spike waveforms, timing of spikes, and number of spikes in response to depolarizing currents, with these properties being different across different birds. This suggests that each bird has uniform HVC_X neuronal intrinsic properties with these features varying from a bird to another. Daou and Margoliash found direct correlation between the intrinsic ion currents properties of HVC_X neurons and the acoustic features that the birds' songs, relating for the first time the molecular properties of ion channels to behavioral measures. While it is known that adult zebra finches sensitivity to auditory feedback decreases with age, this decrease in sensitivity participates in the loss of intrinsic plasticity in adult songbirds. Within each adult zebra finch, HVC_X neurons show intrinsic cellular properties changes when the auditory feedback was altered (Daou & Margoliash, 2020). This underlines the role of HVC_X neurons in learning and memorization of the song (Daou & Margoliash, 2020).

2.2. Synaptic interactions within HVC

One of the touchstone questions that neuroscientists and neurophysiologists studying songbirds are still grappling with are: how are the three classes of neurons in the HVC encode song sequence and phonology and what is the neural basis that's responsible

for orchestrating song and the timing of its syllables? Unveiling what is happening during singing at the level of each population is key for the comprehension of the network operation of this nucleus and for understanding how vocal communication is learned and produced. The correlation among the different HVC neurons population affects the global electrical output of the network; differential activities in neurons could result in firing of action potentials or lack of activity depending on the order of firing of neurons and their connectivity. Therefore, understanding the synaptic connectivity among the three different classes is essential to dissect the network and then build it in biologically plausible ways. Previous studies have shown that both HVC_{RA} and HVC_{X} projecting neurons generate excitatory inputs to HVC_{INT} neurons that are mediated by NMDA and AMPA currents (Mooney & Prather, 2005). In their turn HVC_{INT} neurons inhibit both HVC_{RA} and HVC_{X} via $GABA_A$ and $GABA_B$ synaptic currents (Fig. 5).

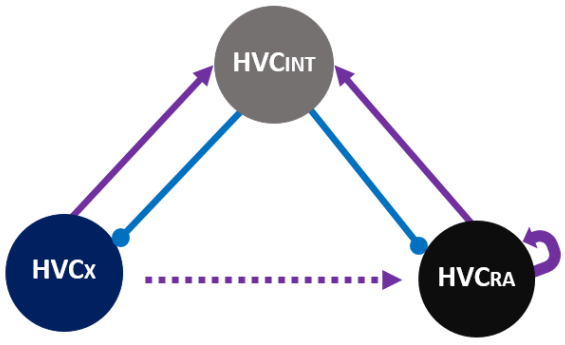

Figure 5: Cartoon diagram showing the synaptic connectivity across the three classes of HVC neurons based on the results of Mooney and Prather (2005) and Kosche et al. (2005). Purple arrows represent excitation via AMPA and NMDA currents. Blue arrows represent inhibition via GABA currents.(Mooney & Prather, 2005). Few monosynaptic connections had been reported between HVC_{RA} and HVC_{X} (dashed arrow).

Mooney and Prather (2005) found only very few monosynaptic connections between HVC_{RA} and HVC_{X}, while mostly it's a di-synaptic inhibition from HVC_{RA} neurons to HVC_{X} neurons via HVC_{INT} neurons; in fact bidirectional synaptic interactions exist between these two categories of HVC neurons in specific reciprocal inhibitory interactions. The patterning activity in HVC is shaped by both inhibitory and excitatory synaptic inputs and the interplay between excitation and inhibition is what enables HVC_{RA}, HVC_{X} and HVC_{INT} neurons to generate their characteristic bursts during singing. Most importantly, inhibitory interneurons is shown to play a major role in song production and are necessary for generating a physiological firing behavior in HVC neurons where absence of this GABA inhibition induces degradation in singing behavior (Kosche *et al.*, 2015). While we know how these three classes of neurons are connected pharmacologically, it remains a blackbox to understand how the neural network within HVC is built to generate the *in vivo* behavior that will be discussed in the very next section.

2.3. HVC neurons activity *in vivo*

In addition to the work done in slice to unveil the pharmacology of the synaptic interactions, a ground breaking result came from the first experiment that was able to record from HVC neurons during singing (Hahnloser *et al.*, 2003). In this study, they showed that HVC_{RA} neurons burst exactly once and at the same exact time during each rendition of the song, HVC_{X} neurons generate 1 to 3 bursts per song, and HVC_{INT} burst densely during singing at a very high frequency (Fig. 6). Similar to HVC_{RA} neurons, evidence showed that HVC_{X} neurons display phase-locked patterns during singing (Fujimoto *et al.*, 2011) although they do not exhibit the same level of stereotypy as HVC_{RA}

neurons. This is the most temporally precise neural sequence known in nature to date (Kozhevnikov & Fee, 2007). This finding questions the reason behind this behavior: what is driving HVC_{RA} and HVC_X neurons to fire with this specific and characteristic patterns that are extremely precise temporally? (Hahnloser *et al.*, 2003). To answer this question we have to understand how the three classes of HVC neurons are connected to generate this behavior.

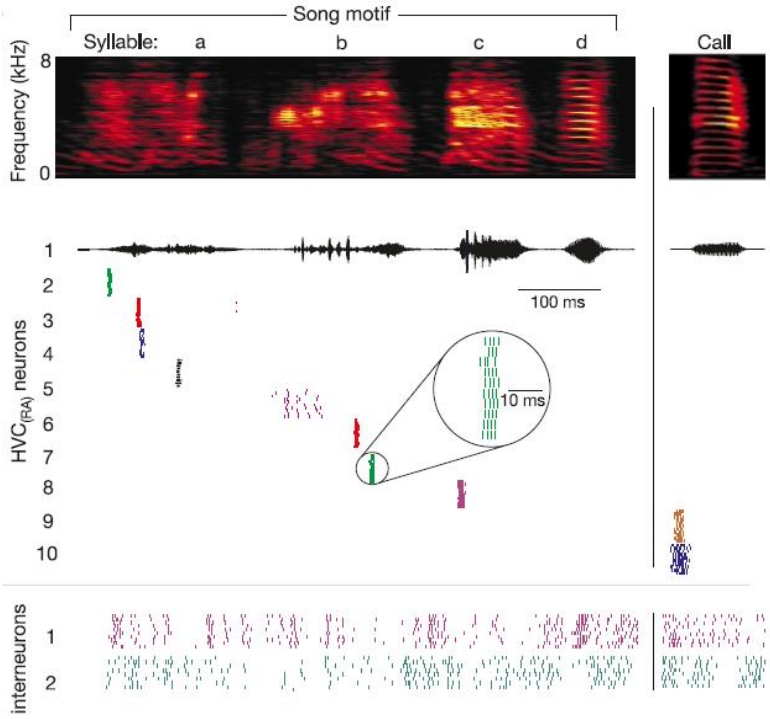

Figure 6: Spike raster plot of ten HVC_{RA} neurons and two HVC interneurons recorded in one bird during singing (left) and call vocalizations (right). Each row of tick marks shows spikes generated during one rendition of the song or call; roughly ten renditions are shown for each neuron. Neural activity is aligned by the acoustic onset of the nearest syllable. HVC_{RA} neurons burst reliably at a single precise time in the song or call; however, HVC interneurons spike or burst densely throughout the vocalizations (Hahnloser et al., 2003).

The extremely sparse and precise patterns of activity in HVC_{RA} neurons could suggest the entire ensemble of HVC_{RA} neurons is functioning to specify the timing of syllables, notes, and even the intervening silent "gaps" between syllables. Indeed, some HVC_{RA} neurons burst during these silences, consistent with this idea (Fig. 6). If the output of the HVC_{RA} ensemble provides a timing signal for song, what and where is the mechanism that determines and sets the song tempo? Based on the observations that RA-projecting HVC neurons generate a single burst of spikes during the song motif and that different neurons appear to burst at many different times in the motif, it has been hypothesized that these neurons generate a continuous sequence of activity over time (Fee *et al.*, 2004; Kozhevnikov & Fee, 2007; Long *et al.*, 2010). In fact, the axons of HVC_{RA} neurons extend local collaterals before exiting HVC, forming excitatory synapses with other HVC_{RA} cells, as well as interneurons and HVC_X cells, providing a potential substrate for a synfire chain (Mooney, 2000; Mooney & Prather, 2005; Mooney, 2009a). In this case, song timing is orchestrated by the propagation of activity through the network like a chain of falling dominoes (Long *et al.*, 2010).

The HVC nucleus requires a relatively long integration time to process auditory feedback of the bird's own vocalizations. Processing auditory information is affected by slow inhibitory mechanisms. In fact, slow hyperpolarizing events have been shown to participate in the necessary inhibition of HVC neurons such as long lasting IPSPs (i.e. GABA mediated) and slow after hyperpolarization requiring action potentials (calcium independent). These events could shape auditory feedback during song learning (Schmidt & Perkel, 1998). In short, despite the key role that HVC plays in the song system, precisely how the neurons in HVC are orchestrating the song sequence and phonology is very poorly

understood. On one level, the "internal anatomy" of HVC neurons and their biophysical properties remained largely undetermined until recently (Daou *et al.*, 2013; Daou & Margoliash, 2020). Without a detailed explanation of the components of the ionic and synaptic currents of HVC neurons and their exact contributions on spike generation, the aim to decode the song is extremely challenging and the story remains incomplete.

2.4. Mathematical modeling of HVC neurons

Each HVC neuronal population has different functional properties and ion channels composition responsible for various responses to depolarizing and hyperpolarizing stimuli. Ionic channels for each neuron type were previously identified using chemical blockers (Daou *et al.*, 2013). In their work, Daou et al (2013) also developed a biophysically realistic model that was tuned to fit the biological data they generated *in vitro*, incorporating the ionic currents that were identified pharmacologically. The Daou et al 2013 model incorporated the potassium (I_K) and sodium (I_{Na}) currents as spike generating currents, a high threshold L-type calcium current (I_{CaL}), a low threshold T-type calcium current (I_{CaT}), a small conductance calcium activated potassium current (I_{SK}), a persistent sodium current (I_{Nap}), a sodium dependent potassium current (I_{KNa}), an A type potassium current (I_A), a hyperpolarization current (I_h) and a leak current (I_L). These currents were shown to be the main players in orchestrating the HVC neuronal firing patterns (Daou et al., 2013).
The membrane potential of every HVC neuron obeys the following equation:

$$C_m \frac{dV}{dt} = -I_L - I_K - I_{Na} - I_{CaL} - I_{CaT} - I_A - I_{SK} - I_{KNa} - I_h - I_{Nap} + I_{app}$$

where C_m is the membrane capacitance and I_{app} the magnitude of the applied current.

While all model neurons share the same ionic currents, there are some differences however in the ionic currents' magnitudes across the three classes of HVC neurons. For example, HVC interneurons that lack the adaptation feature have a very small I_{SK} and I_{KNa} currents, while in return they exhibit a much stronger I_K and I_h currents than the other two classes of projecting neurons. RA-projecting neurons seem to be the only class of neurons that exhibit a strong A-type K^+ conductance due to the delay to first spike feature that they exhibit solely. Moreover, X-projecting and interneurons are the only neurons that exhibit I_h and I_{CaT} currents because they are the only neurons that exhibit a sag and rebound firing in response to negative current pulses. The model responses and fits are shown in Fig. 7.

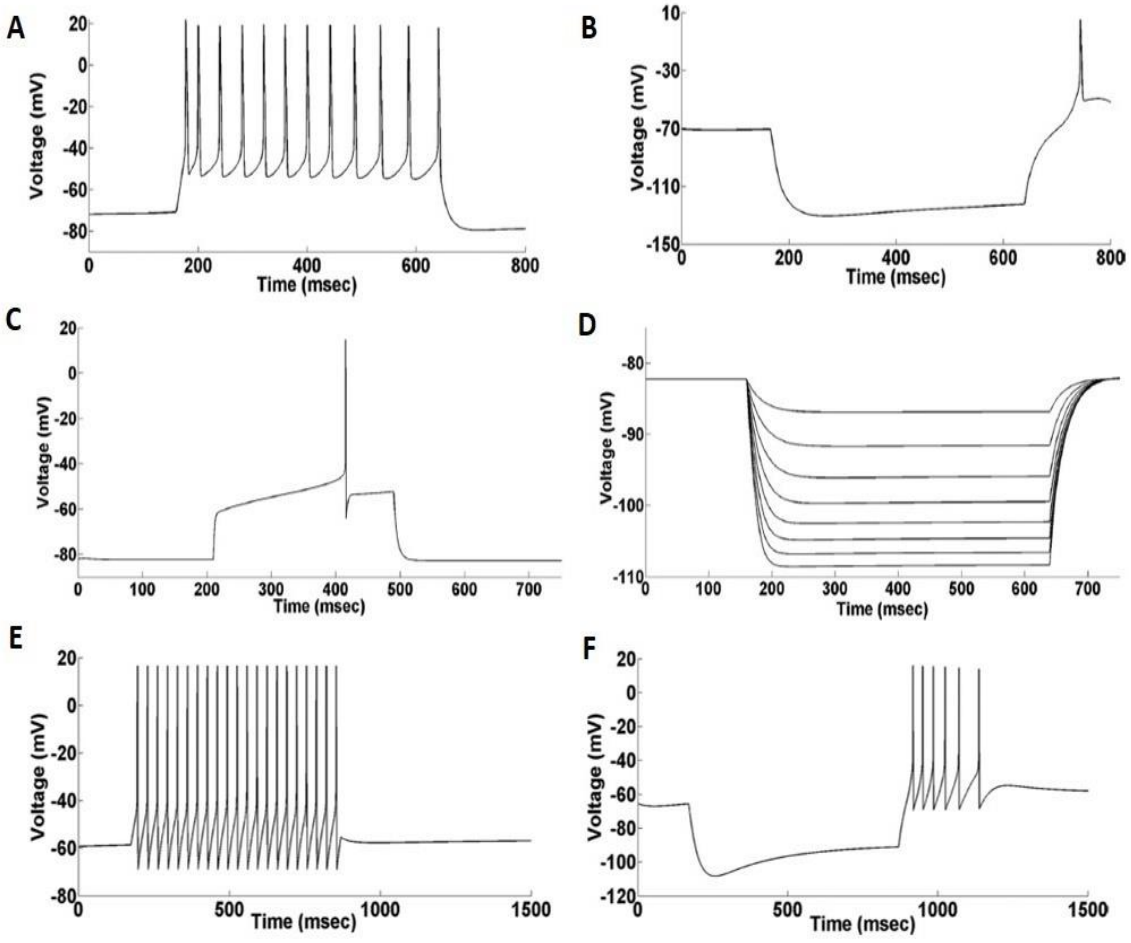

Figure 7: Mathematical model simulations of HVC neurons. A: HVC_X model neuron parameters were calibrated to match the voltage traces of a depolarizing pulse of 100 pA. B: Model HVC_X neuron exhibiting a weak sag in response to negative current pulses (compare Fig. 7A-B to Fig. 7A-B). C: HVC_{RA} model neuron parameters were calibrated to match the experimental recording (I_{app} = 150 pA). The long delay to spiking is due to the A-type K current (I_A). D: For the same parameter values used in C, the HVC_{RA} model neuron has no sag but exhibits inward rectification in the spacing between voltage traces (compare Fig. 7C-D to Fig. 7C-D). E: HVC_{INT} model neuron exhibiting high firing frequency with no adaptation in response to 75 pA current pulse. F: The same model HVC_{INT} neuron exhibiting prominent sag and strong rebound burst in response to negative current pulses (compare Fig. 7E-F to Fig. 7E-F).

Other models of how neurons, in the HVC nucleus, might be organized and interconnected have been proposed (Troyer & Doupe, 2000; Drew & Abbott, 2003; Abarbanel *et al.*, 2004a; Abarbanel *et al.*, 2004b; Mooney & Prather, 2005; Li & Greenside, 2006; Jin *et al.*, 2007; Katahira *et al.*, 2007; Gibb *et al.*, 2009a; b; Jin, 2009; Long *et al.*, 2010; Cannon *et al.*, 2015). These models were designed in the aim to reproduce the observed sparse bursting of HVC_{RA} neurons (Hahnloser *et al.*, 2003). Some models invoked a feed-forward chain of excitation (Li & Greenside, 2006; Gibb *et al.*, 2009b; Long *et al.*, 2010; Cannon *et al.*, 2015). Gibb et al. 2009 was the first to develop a computational model of birdsong sequencing. Their model, though non-biologically realistic, hypothesized for the first time that different networks in HVC control different syllables production, that HVC_{INT} provide mutual inhibition between networks controlling syllables, and that these syllable networks are sequentially excited by neural feedback via the brain stem or a similar feedback pathway (Gibb *et al.*, 2009a). In a subsequent work, they showed that the sparse bursting seen in projecting neurons is generated in bistable groups of recurrently connected HVC_{RA} neurons with the inhibitory interneurons terminating bursts in the HVC_{RA} groups (Gibb *et al.*, 2009a). In a nutshell, their model is based on the observation made by Hahnloser et al. 2002 that HVC_{RA} neurons exhibit sparse bursting and that these neurons form a chainlike organization in which neurons burst in sequence at every moment of the song (Hahnloser *et al.*, 2003; Gibb *et al.*, 2009a).

Armstrong and Abarbanel (Armstrong & Abarbanel, 2016; Armstrong, 2018) proposed an alternative to the HVC chain model. Their model was based on the biophysical process of mutual inhibition between interneurons. The HVC was modeled as several functional HVC units (FHU). In each FHU, three HVC_{INT} neurons were connected all-to-

all, and each interneuron synaptically inhibits two of three HVC_{RA}. An HVC unit is capable of displaying multiple modes of activity, depending on the connection strengths among the HVC_{INT} neurons. Plus, each syllable-gap pair was assigned a distinct FHU. Based on the identity of the neurons that are firing at a specific time, they suggested that a different set of RA neurons will be recruited; the group of RA neurons selected will then dictate the behavior of the brainstem regions controlling the driving forces of the song. Finally, the HVC FHUs activity is controlled by a recurrent feedback from the brainstem. Despite the fact that this model was able to replicate the sequential propagation within HVC_{RA} neurons, their model disregarded principal ionic currents that were found to participate in HVC neurons activity. Not to mention that for the sake of simplicity, brainstem regions cross-connectivity was omitted from this model adding a non-realistic assumption to their model (Armstrong & Abarbanel, 2016; Armstrong, 2018).

2.5. Aim of the study

Despite the instructive nature of all the previously developed computational models, all of these models have failed to capture the intricate details of spike morphology, failed to incorporate the right ionic currents that exist biologically, or failed to generate the same patterns seen *in vivo*. The aim of this study is to develop a computational neural network model of HVC_{RA}, HVC_X and HVC interneurons that could replicate the *in vivo* behavior of these neurons during bird singing while incorporating all ionic and synaptic currents that we know exist for the classes of HVC neurons and their network (Daou *et al.*, 2013; Daou & Margoliash, 2020).

In order to achieve this goal, we decided to do the following: 1) replicate the experimental results of the *in vitro* firing patterns of each HVC neurons population separately (Daou *et al.*, 2013; Daou & Margoliash, 2020), then 2) replicate the experimental results of the *in vitro* study that unveiled the pharmacological nature of the synaptic connectivity across the three classes of HVC neurons (Mooney & Prather, 2005) and which explored the synaptic basis of the HVC microcircuit, and finally, 3) to design plausible neural networks incorporating all classes of HVC neurons that are able to replicate the *in vivo* firing patterns of HVC neurons during singing (Hahnloser *et al.*, 2003; Fujimoto *et al.*, 2011).

In order to build the desired networks, we decided to create different scenarios of network architectures that could possibly generate the *in vivo* responses during singing. Our goal is not to isolate the best network architecture, but to explore different possible realistic scenarios in which the different types of HVC neurons can interact to produce the stereotyped HVC_{RA} and HVC_X sequences.

CHAPTER 3

MATERIALS & METHODS

Based on previous studies in neural computational modeling (Daou *et al.*, 2013), a multiple compartment conductance based biophysical model of HVC neurons has been developed. Model simulations were performed using Matlab (Math-Works). For modeling HVC neurons, we used Hodgkin-Huxley models with additional synaptic currents added to reproduce biological features of the voltage traces observed *in vivo*. Every model neuron is represented by ten ordinary differential equations for the different state variables. The activation/inactivation functions and time constants were based on previous mathematical neural models (Hodgkin & Huxley, 1952; DestexheCA & Babloyantz, 1993; Terman *et al.*, 2002; Wang *et al.*, 2003; Dunmyre *et al.*, 2011; Daou *et al.*, 2013). Synaptic currents are very essential in multi-compartment modeling to ensure interconnectivity between different neurons types. The synaptic currents and corresponding neurotransmitters are based on Mooney et al 2005 study in which they examined the interaction between HVC_{RA}, HVC_{X} and HVC_{INT} neurons. The majority of our fitting parameters were maximum conductance and synaptic strengths which usually vary across neurons classes.

The membrane potential of each HVC neuron obeys the following equation:

$$C_m \frac{dV}{dt} = -I_L - I_K - I_{Na} - I_{CaL} - I_{CaT} - I_A - I_{SK} - I_{KNa} - I_h - I_{Nap} + I_{app}$$

where C_m is the membrane capacitance and I_{app} the magnitude of the applied current. The included ionic currents were pharmacologically identified by Daou et al. 2013 .While all

model neurons share the same ionic currents, the ionic currents' magnitudes vary across the classes of HVC neurons. The voltage dependent ionic currents' equations are modeled as follows:

$$I_K = g_K n^4 (V - V_K)$$

$$I_{Na} = g_{Na} m_\infty^3(V) h (V - V_{Na})$$

$$I_{Nap} = g_{Nap} mp_\infty(V) hp (V - V_{Na})$$

$$I_A = g_A a_\infty(V) e (V - V_K)$$

$$I_{CaL} = g_{CaL} V s_\infty^2(V) \left(\frac{Ca_{ex}}{1 - e^{\frac{2FV}{RT}}}\right)$$

$$I_{CaT} = g_{CaT} V [a_T]_\infty^3(V) [b_T]_\infty^3(r_T^A) \left(\frac{Ca_{ex}}{1 - e^{\frac{2FV}{RT}}}\right)$$

$$I_{SK} = g_{SK} k_\infty([Ca^{2+}]_i)(V - V_K)$$

$$I_{KNa} = g_{KNa} w_\infty([Na^+]_i)(V - V_K)$$

$$I_h = g_h[k_r r_f + (1 - k_r) r_s](V - V_h)$$

$$I_L = g_L(V - V_L)$$

where n, m, h, e, hp, $a_{T\infty}$, $b_{T\infty}$, k_∞, m_∞, mp_∞, a_∞ and s_∞ are the gating variables.

While for the synaptic currents, the model equations are the following:

$$I_{AMPA} = \overline{g_{AMPA}} s (V - V_{AMPA})$$

$$I_{NMDA} = \overline{g_{NMDA}} s\, B(V)(V - V_{NMDA})$$

$$I_{GABA-A} = \overline{g_{GABA-A}} s (V - V_{GABA-A})$$

where s satisfies $[T]_{pre} = \frac{T_{max}}{1 + \exp(-\frac{(V_{pre} - V_T)}{K_p})}$ and $\frac{ds}{dt} = a_r[T](1 - s) - a_d s$

and $B(V) = \frac{1}{1 + \frac{\exp^{-0.062V}[Mg^{2+}]}{3.57}}$ represents the magnesium block.

Parameter	Value	Parameter		Value
V_K	-90 mV		V	0 mV
V_{Ca}	80 mV		a_r	1.1 $mM^{-1}.ms^{-1}$
V_{Na}	70 mV		a_d	0.19 ms^{-1}
V_h	-30 mV		V	-80 mV
V_L	-70 mV		a_r	5 $mM^{-1}.ms^{-1}$
Ca_{ex}	2.5 mM		a_d	0.18 ms^{-1}
$\frac{F}{RT}$	26.7 mV^{-1}	HVC_{RA}	k_r	0.95
T_{max}	1 mM		C	20 pF
V_T	2 mV	HVC_X	k_r	0.3
K_p	15 mV		C	100 pF
		HVC_{INT}	k_r	0.01
			C	75 pF

Table 1: Constant model parameters.

We present four network architectures with the aim to replicate *in vivo* firing patterns of HVC neurons. AMPA and $GABA_A$ synaptic currents where used to connect neurons inside each architecture based on the pharmacological dual synaptic connections as described by Mooney & Prather (Mooney & Prather, 2005). The synaptic conductances values ranges are summarized in Table 2.

Synaptic conductance		Values range (nS)
g_{AMPA}	HVC_{RA} to HVC_{RA}	10 – 40
	HVC_{RA} to HVC_{INT}	80 – 300
	HVC_X to HVC_{RA}	30
$g_{GABA\text{-}A}$	HVC_{INT} to HVC_X	50 – 1500
	HVC_{INTA} to HVC_{INTB}	200
	HVC_{INTB} to HVC_{RA}	200

Table 2: Dual synaptic conductances values.

In the fourth network architecture (Fig. 21), a random assignment of HVC_{RA} neurons was established as follows: a gap of 10 HVC_{RA} neurons was sufficient to generate non overlapping bursts in a chosen interneuron. This assignment was based on the observation that HVC_{RA} neurons propagate bursting activity very fast. This induces bursts overlapping in HVC interneurons which destroys their bursting pattern, for example, in case the interneuron receives two excitatory inputs within few milliseconds. Furthermore, if an HVC_X neuron is inhibited from several consecutive HVC_{INT} bursts that are very close in time, this ruins the HVC_X bursts' shape or delays its rebound bursting. Thus, we ensured that the random assignment of HCV_{RA} neurons to each HVC_{INT} will be able to generate realistic bursts that are fairly spaced in time, in both HVC interneurons and HVC_X neurons. For instance, HVC_{INT}^{1} could be assigned randomly HVC_{RA}^{1}, HVC_{RA}^{11}, HVC_{RA}^{21}, HVC_{RA}^{31}, HVC_{RA}^{41}, HVC_{RA}^{51}, similarly for HVC_{INT}^{2} being assigned randomly another set of HVC_{RA}

neurons distant of 10 neurons and so on. Thus, each HVC_{INT} neuron receives between 3 to 6 excitatory AMPA synapses from the group of HVC_{RA} neurons that was assigned to it.

To address the sparse firing of interneurons, making their activity more biologically realistic, we injected in the model neurons a stochastic input current. The stochastic input current was added in the differential equation dictating the membrane potential of the model neuron. The constant DC applied current I_{app} was replaced by a random number that can take any integer value up to 150 pA. In other words, at each instant in time in the simulation, a random number for the applied current was applied to the model neuron. Injecting the stochastic input inside the differential equation implies that the value of the applied current varies at a millisecond timescale. For instance, for a simulation of 1 second or 1000 milliseconds (typical duration of a song motif), with a time step of 0.1, 10000 data points will be generated meaning that 10000 different values for the applied current will be applied to the neuron for the running simulation. The ability of the model architecture to reproduce the sequential propagation in presence of this stochastic input constitutes an indicator of the robustness of the model.

CHAPTER 4

RESULTS

Understanding the synaptic connectivity between the different classes of HVC neurons is key for building a more complex network of these neurons.

4.1. Replicating the dual synaptic connectivity patterns.

Using intracellular recordings from pairs of identified HVC neurons in brain slices, Mooney and Prather (2005) assessed the synaptic connections within the HVC microcircuit. They found extremely robust disynaptic feedforward inhibition from HVC_{RA} to HVC_X neurons (via HVC_{INT} neurons), strong monosynaptic excitation from HVC_{RA} and HVC_X to HVC_{INT} neurons (via NMDA and AMPA currents) as well as strong monosynaptic inhibition from HVC_{INT} neurons to HVC_{RA} and HVC_X (via $GABA_A$ and $GABA_B$ currents).

DC-evoked action potentials in the HVC_{RA} neuron triggered an inhibitory postsynaptic potential (IPSP) in the HVC_X neuron (Fig. 8A1, (Mooney & Prather, 2005)). Model HVC neurons were connected in a network to replicate the same responses. In particular, one HVC_{RA} neuron was connected to excite one HVC_{INT} neuron via NMDA and AMPA currents, with the interneuron in return inhibiting an HVC_X neuron via $GABA_A$ and $GABA_B$ currents (Fig. 8A2). Similarly, DC- evoked action potentials in the HVC_{RA} neuron evoked a fast depolarizing postsynaptic potential (dPSP) in the corresponding HVC_{INT}

neuron (Fig. 8B1, (Mooney & Prather, 2005)). Model parameters were fit to replicate the same firing patterns in an HVC_{RA} to HVC_{INT} connection (Fig. 8B2).

Similarly, DC-evoked action potentials in HVC_{INT} neurons generate fast IPSPs in HVC_X neurons (Figs. 9A1, B1). Model HVC_{INT} and HVC_{RA} neurons were connected and simulated to generate similar responses (Figs. 9A2, B2). Again, the difference between panels in A and B are the stimulus waveforms. Notice that both biological as well as model HVC_X neurons in panels B1-B2 exhibit a ramp up in the voltage trace in response to the inhibition from HVC_{INT}, primarily due to the I_h current. Finally, the HVC_X to HVC_{INT} excitatory PSPs (Fig. 9C1) was replicated (Fig. 9C2) similarly.

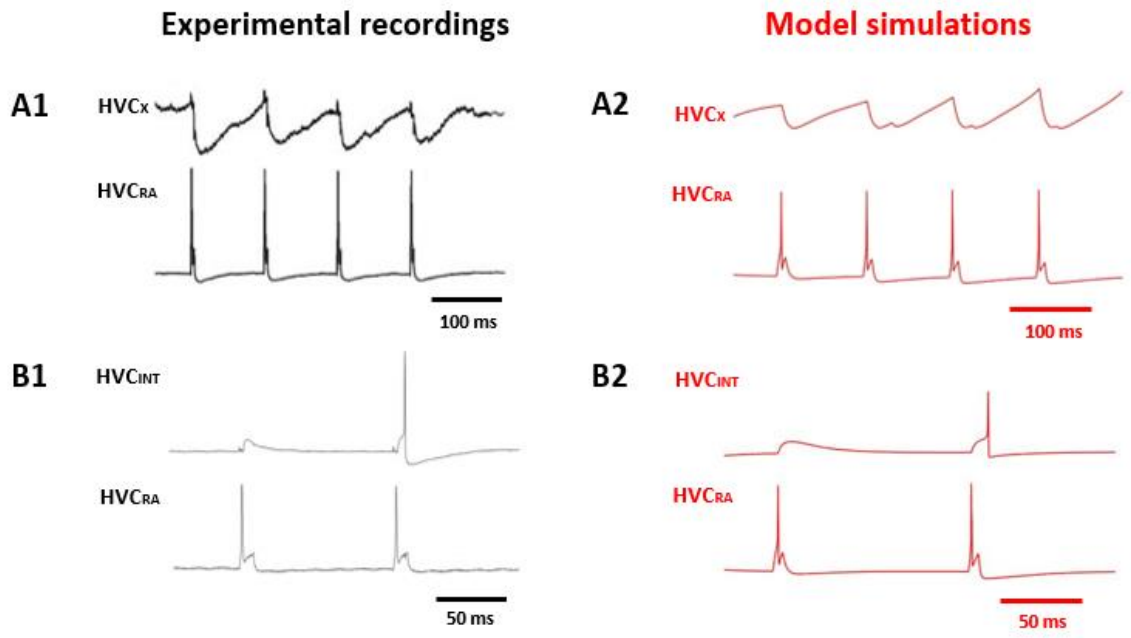

Figure 8: Model output compared to experimental results obtained by Mooney et al. 2005 (Mooney & Prather, 2005). A1: HVC_{RA} to HVC_X connectivity as seen in experimental recordings. A2: HVC_{RA} to HVC_X model connectivity; a depolarizing current of 500 pA was applied to HVC_{RA} for 500 ms. B1: HVC_{RA} to HVC_{INT} connectivity as seen in experimental recordings. B2: HVC_{RA} to HVC_{INT} model connectivity. A depolarizing current of 200 pA was applied to HVC_{RA} for 500 ms.

The fitting and calibration of the three model HVC neurons designed above gave us confidence to go further and start our neural networks design to generate the *in vivo* behavior because now our networks are based on biologically realistic parameters and data. In order to build the desired networks, we decided to create different scenarios of network architectures that could possibly generate the *in vivo* responses during singing. We believe that the simulation of different models is able to enlighten us about the biological model structure, which could perhaps be then tested and verified.

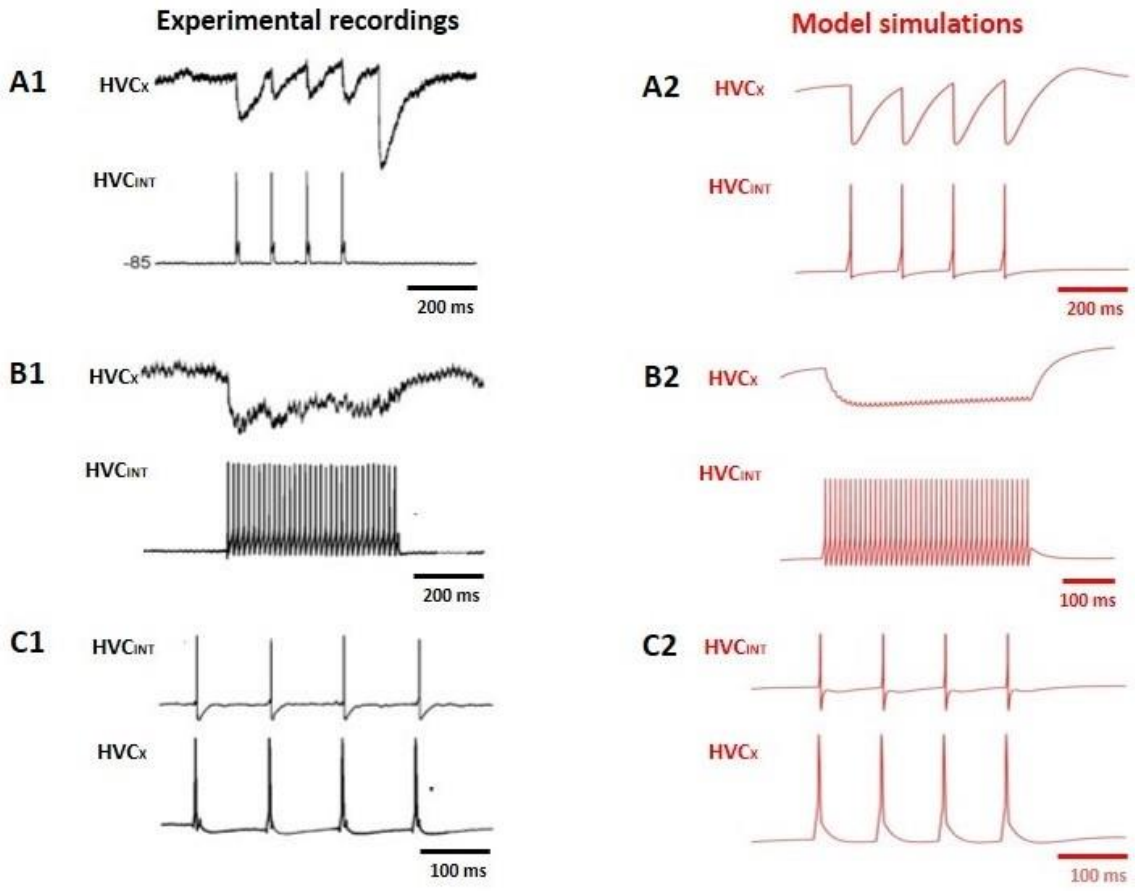

Figure 9: Model output compared to experimental results obtained by Mooney et al. 2005(Mooney & Prather, 2005). A1: HVC_{INT} to HVC_X connectivity as seen in experimental recordings. A2: HVC_{INT} to HVC_X model connectivity; a depolarizing current of 200 pA was applied to HVC_{INT}. B1: HVC_{INT} to HVC_X connectivity as seen in experimental recordings.B2: HVC_X to HVC_{INT} model connectivity. A depolarizing current of 200 pA was applied to HVC_{INT} for 500 ms. C1: HVC_X to HVC_{INT} connectivity as seen in experimental recordings. C2: HVC_X to HVC_{INT} model connectivity. A depolarizing current of 1000 pA was applied to HVC_X.

CHAPTER 5

NEURAL NETWORKS DESIGN

Chromophore-targeted neuronal degeneration, a procedure that biophysically induces apoptotic death in specific neuron populations (Macklis, 1993; Madison & Macklis, 1993; McConnell, 1995), had been previously applied on HVC neurons to test whether the neuronal death of specific classes of HVC neurons have any effect on song generation (Scharff *et al.*, 2000). The results of that study, which remains very controversial in the field till nowadays, showed that adult song production was not affected by the targeted elimination of HVC_X neurons, but the elimination of HVC_{RA} neurons induced song deterioration. Other studies nevertheless contradicted the Scharff et al (2000) results and showed that the HVC_X neuronal population is an essential element for both song production and learning (Mooney, 2009; Bolhuis *et al.*, 2012; Roberts *et al.*, 2017; Daou & Margoliash, 2020). Given these different results in mind, we designed several neural networks incorporating different combinations of these classes of HVC neurons but that are able to generate the *in vivo* firing patterns seen during singing (Hahnloser *et al.,* 2003; Fujimoto *et al.,* 2011).

In this study, we present network architectures that show how the sequential activity in the HVC projection neurons can propagate. The prototype networks are composed of chains of HVC microcircuits, each with its own intrinsic dynamics. Each mean field neuron in a microcircuit is representative of a neural population. We envision the HVC to be

composed of many copies of such microcircuit chains that are associated with syllables with roughly synchronized activity (Fee *et al.*, 2004).

5.1. Network 1: RA-projecting neurons driven activity

The first network architecture is the simplest architecture illustrated in Fig. 10. In this network, sequential activity propagates solely across HVC_{RA} neurons in a synfire chain mode. In this chain model, burst timing is controlled by a synaptic input from a preceding group of HVC_{RA} neurons connected via AMPA currents. The stable propagation of bursts requires precisely tuned synaptic strengths to avoid runaway excitation or decay. It has been proposed that sequential states of neural activity may be generated by synaptically connected chains of neurons (Amari, 1972; Abeles, 1991; Mauk & Buonomano, 2004). In this view, activity propagate through the HVC network - like a chain of falling dominoes - forming the basic clock that underlies song timing (Long *et al.*, 2010).

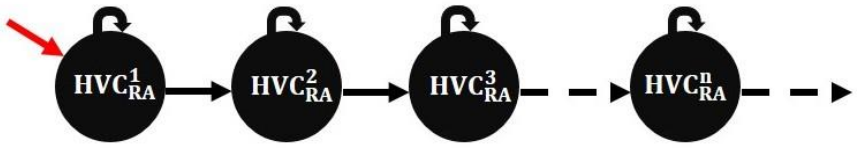

Figure 10: Network 1 design structure. Black arrows symbolize excitation via AMPA currents. The red arrow onto HVC_{RA}^{1}represents the excitatory drive (DC current) from outside the HVC.

The activity patterns that this network displays are shown in Fig. 11. Only HVC_{RA}^{1} neuron receives a DC pulse to kick start the network mimicking the excitatory drive that HVC_{RA} neurons receive from ascending auditory nuclei. The spiking in HVC_{RA}^{1} is amplified by the excitatory projection back onto HVC_{RA}^{1}. This positive feedback results in a burst of HVC_{RA}^{1} activity, which generates a burst of activity in HVC_{RA}^{2} due to excitatory AMPA/NMDA coupling. Intracellular Ca^{2+} accumulates during the burst. This result in a buildup of Ca^{2+}-activated K^{+} current (I_{SK}) that terminates the burst. The burst in HVC_{RA}^{2} propagates to HVC_{RA}^{3} in a similar fashion and so on. In this and some other subsequent networks presented, the reason only one microcircuit receives DC pulse (instead of all other networks) from outside HVC is to have the sequential activity propagation solely dependent on HVC neurons themselves instead of extra-nucleus factors, thereby having HVC the sole orchestrator of the neural sequence.

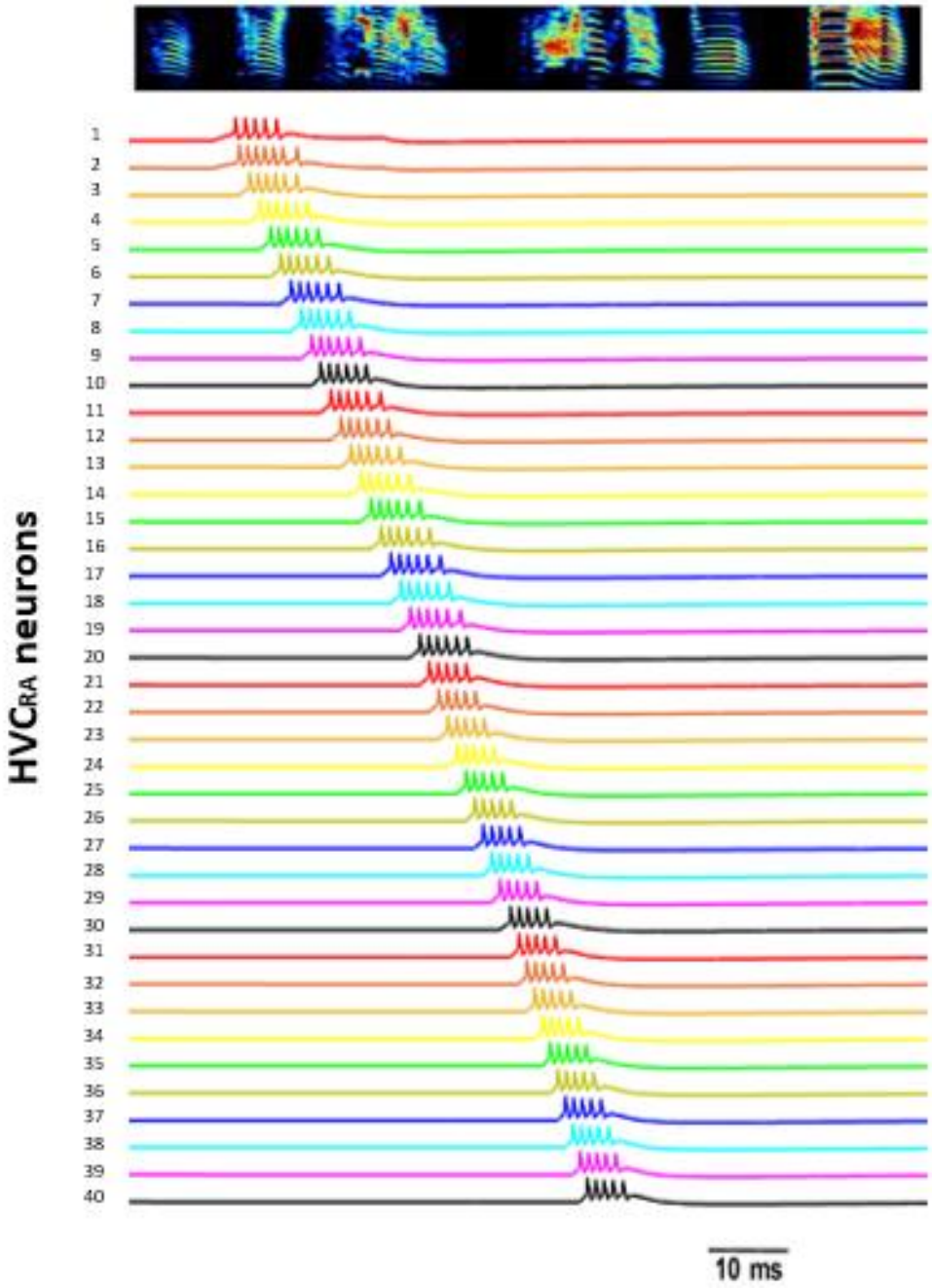

Figure 11: HVC_{RA} spiking patterns of network architecture one. Sequential bursting of 40 different HVC_{RA} neurons (labeled with numbers) showing the propagation of sequential activity independent of HVC_X and HVC_{INT} neurons. The neural traces are aligned by the acoustic elements of a spectrogram from a bird's song illustrating the firing of HVC_{RA} neurons with respect to ongoing song.

The duration between the burst of one HVC_{RA} neuron and the burst in the next HVC_{RA} neuron in the chain is ~ 5 ms (Fig. 12). This duration of time is solely dependent on the strength of the synaptic conductance that connects the two neurons in the chain. The strength of the burst and the number of spikes in the burst of any HVC_{RA} neuron are dependent on the strength of the synaptic conductance from that HVC_{RA} neuron onto itself, as well as the build-up of intracellular Ca^{2+} during the burst inside the HVC_{RA} neuron that results in a stronger I_{SK} conductance that truncates the burst shorter.

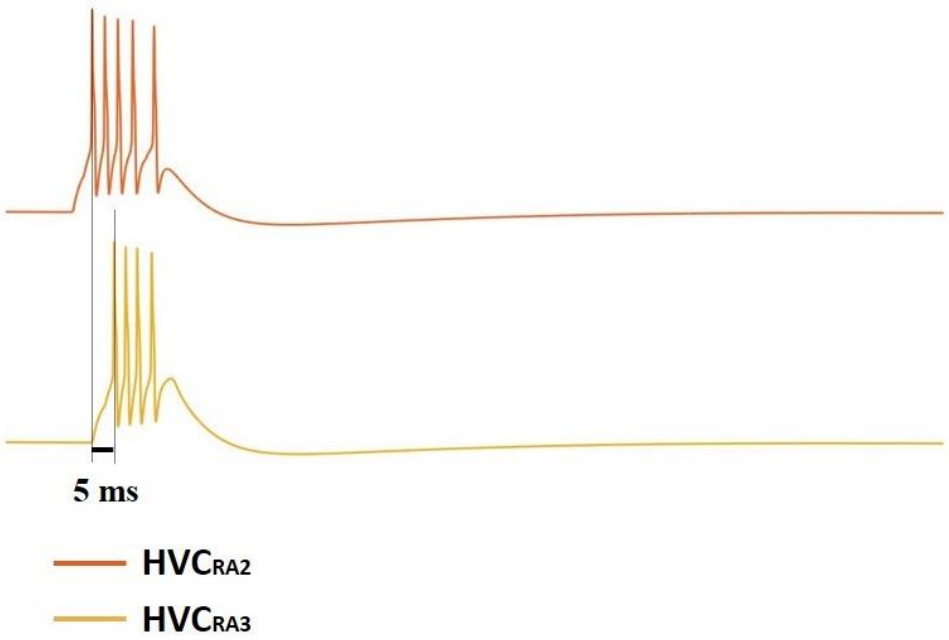

Figure 12: Firing patterns of two sample HVC_{RA} neurons (HVC_{RA}^{2} and HVC_{RA}^{3}) in the chain. The duration between the burst of one HVC_{RA} neuron and the burst in the next HVC_{RA} neuron in the chain is ~ 5 ms. This duration of time is solely dependent on the strength of the synaptic conductance that connects the two neurons in the chain.

Although this network produces the desired behavior of HVC_{RA} neurons, one main drawback is that it disregards the HVC_X and HVC_{INT} neuronal populations. However, few research groups believe that the orchestration of HVC_{RA} neurons *in vivo* is driven solely by HVC_{RA} neurons themselves (Scharff *et al.*, 2000; Fee *et al.*, 2004; Long *et al.*, 2010), and this network was designed to support this idea and show that sequence propagation can be generated with HVC_{RA} neurons solely.

5.2. Network 2: Interneurons-HVC_{RA} interaction to propagate activity

We next consider architecture Fig. 13, which gives more complex network dynamics than the previous network incorporating HVC interneurons into the equation. Previous studies have showed that there exists two classes of HVC interneurons based on the straining protocols conducted (Wild *et al.*, 2005) and that exhibit different electrophysiological features (Gulyás *et al.*, 1996; Gritti *et al.*, 2003). To this end, we designed a network that incorporates two classes of interneurons, classes A and B, as well as RA-projecting neurons. We assume that neurons of the HVC that are involved in the timing of syllables form microcircuits. Each microcircuit contains subpopulations of HVC_{RA} and the two classes of HVC_{INT} neurons. The many neurons within a subpopulation are assumed to be electrically active at the same time, so we represent this subpopulation by a single representative neuron. For example, the RA-projecting subpopulation in a microcircuit is represented by the model neuron HVC_{RA}. The representative neurons are then synaptically coupled together to form a microcircuit, or to project to another microcircuit as a connecting link in the microcircuit chain.

Within each of the microcircuits in Fig. 13 (the first of which is enclosed by a dashed rectangle), there are excitatory projections from HVC_{RA} back onto HVC_{RA}, inhibitory projections from HVC_{INTA} to HVC_{INTB} as well as from HVC_{INTB} to HVC_{RA}. The microcircuits interact with each other via the projections from HVC_{RA} from one microcircuit to HVC_{INTA} in a following microcircuit.

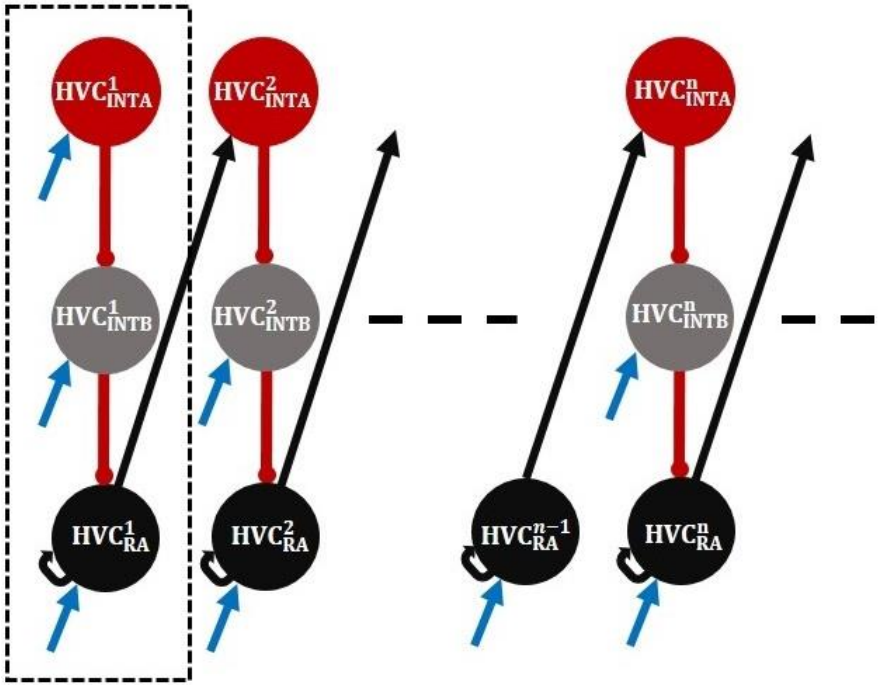

Figure 13: Arrangement of prototype network architecture two. Two classes of HVC_{INT} neurons are presented (HVC_{INTA} in red and HVC_{INTB} in grey). Black arrows symbolize excitation via AMPA currents. Red arrows (with circle heads) symbolize inhibition via GABA currents. Blue arrows symbolize excitatory drive (DC inputs) from outside the HVC. The first microcircuit is enclosed by a dashed rectangle to represent its role as a leading microcircuit in the network.

Each HVC^{i}_{INTA} neuron inhibits an HVC^{i}_{INTB} neuron via GABA currents, and HVC^{i}_{INTB} neuron in its turn inhibits HVC^{i}_{RA} via GABA currents as well. HVC^{i}_{RA} neurons excites HVC^{i+1}_{INTA} in the next microcircuit via AMPA and NMDA currents to ensure

propagation of the pulse through the subsequent microcircuit. We refer to each group of one HVC_{INTA}, one HVC_{INTB} and one HVC_{RA} as a microcircuit. Each HVC_{RA} neuron receives excitatory drive (DC current) from outside the HVC (upward blue arrows in diagram).

The activity patterns that this network displays are shown in Fig. 14. Among class A interneurons, only HVC^{1}_{INTA} neuron receives a DC pulse to kick start the network, representing the incoming input from outside HVC. All class B interneurons however receive a DC pulse to be able to spike consistently during the song. While for HVC_{RA} neurons, bursting requires a DC input to each of them along with AMDA/NMDA excitation from HVC^{i}_{RA} to itself. When HVC^{1}_{INTA} receives the driving input, it fires several spikes (Fig. 14A). This firing silences HVC^{1}_{INTB} due to GABA inhibitory coupling (Fig. 14B). Now, HVC^{1}_{RA} , that was prohibited from firing due to HVC^{1}_{INTB} continuous inhibition, escapes the inhibition and generate a burst of activity (Fig. 14C). The spiking in HVC^{1}_{RA} is amplified by the excitatory projection back onto HVC^{1}_{RA}. HVC^{1}_{RA} in its turn generate a burst in HVC^{2}_{INTA} in the second microcircuit due to excitatory AMPA/NMDA coupling. In particular, HVC^{1}_{RA} generates a burst of activity in HVC^{2}_{INTA} due to strong excitatory AMPA/NMDA drives, which then in its turn carries the chain of activity across HVC^{2}_{INTB} and HVC^{2}_{RA} in a similar fashion to the first microcircuit.

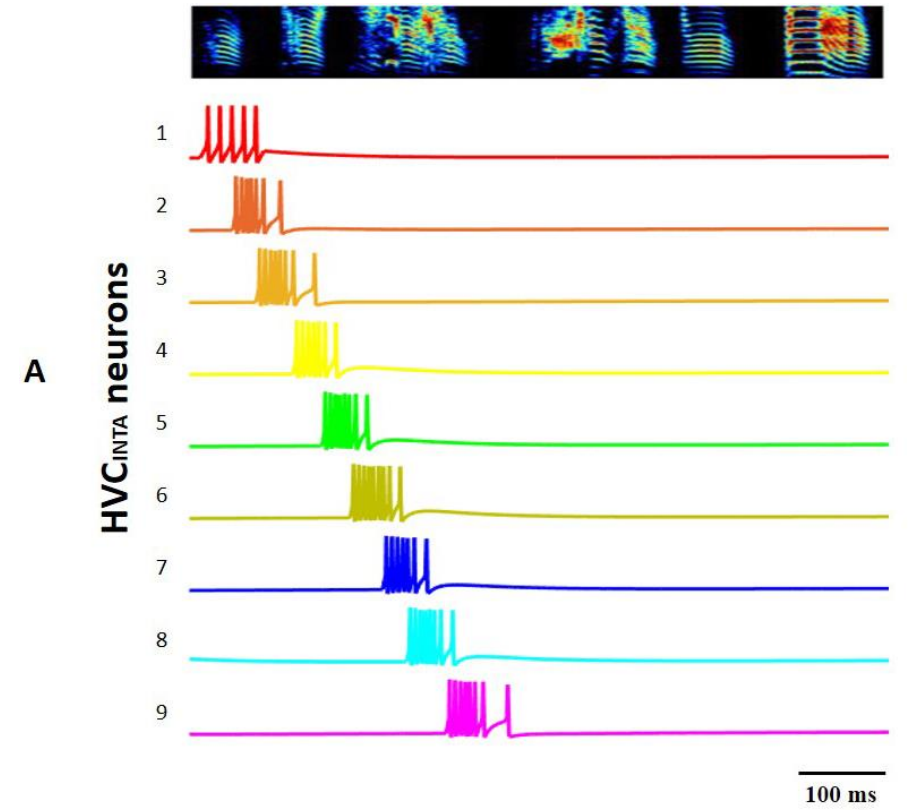
A
HVCINTA neurons
1
2
3
4
5
6
7
8
9
100 ms
B
HVCINTB neurons
1
2
3
4
5
6
7
8
9
100 ms

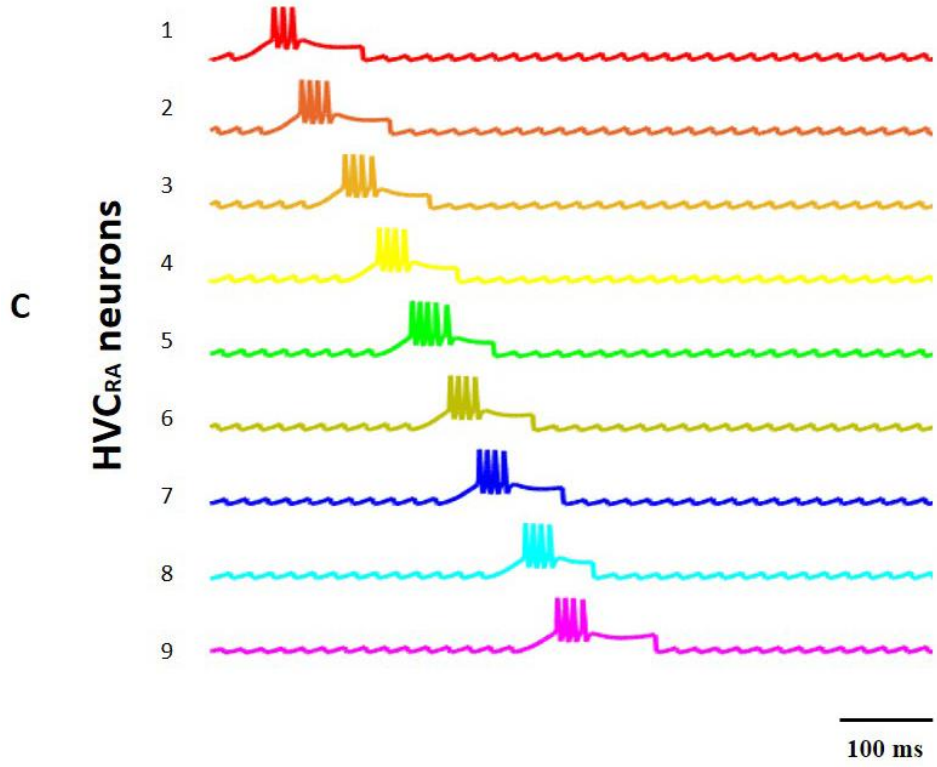

Figure 14: HVC spiking patterns of network architecture two. Class A and class B HVC interneurons firing pattern shown in panels A and B respectively. Class B interneurons fire continuously except at particular instances of time when they are inhibited by Class A interneurons. C: Sequential bursting of HVC_{RA} neurons within the network.

The strength and duration of the burst in HVC_{INTA} neurons is controlled by the strength of the synaptic input from HVC_{RA}^{i} to HVC_{INTA}^{i+1}. The duration of HVC_{RA} bursts is determined by two factors. The first is the rate of Ca^{2+} accumulation, which results in accumulation of the hyperpolarizing SK current. The second is the strength and duration of the inhibition HVC_{INTB}^{i} neurons received from HVC_{INTA}^{i} neurons (the longer/stronger the inhibition of HVC_{INTB}^{i}, the longer the HVC_{RA}^{i} bursts). This activity propagates throughout the chain of microcircuits causing a sequence of HVC_{RA} bursts (Fig. 14).

Spike raster plot of HVC_{RA} neurons are shown in Fig. 15. Each row of tick marks shows the spikes generated during one rendition of the song with each rendition being modeled as starting the simulations from a different set of initial conditions for the state variables. Roughly ten renditions are shown for each neuron (zoomed stack of tick marks). Neural activity, aligned by the acoustic onset of the nearest syllable, shows how HVC_{RA} neurons could burst reliably at a single precise time in the song (Fig. 15). Moreover, these activity patterns that this network exhibit show that it is a robust network because starting the simulations from different initial conditions for the state variables does little to no effect to the timing of spiking.

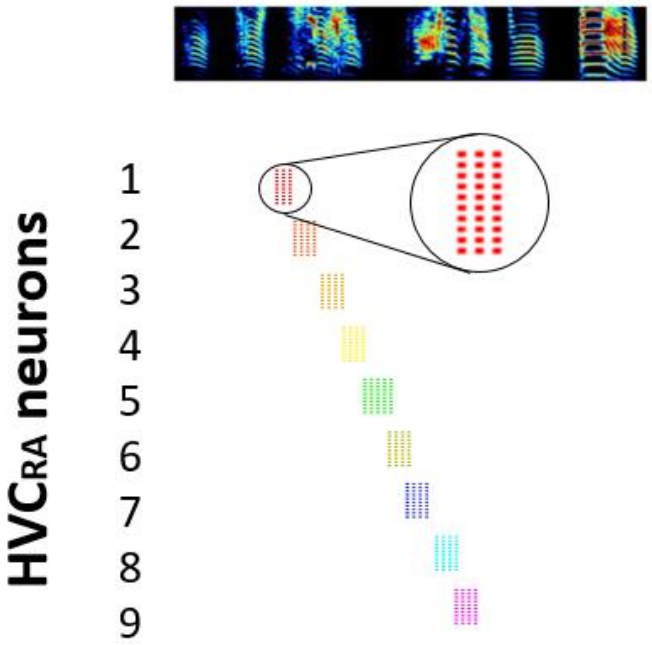

Figure 15: Spike raster plot of HVC_{RA} neurons showing the time locked firing of neurons relative to vocalizations. Each row of tick marks shows spikes generated during one rendition of the song or call; roughly ten renditions are shown for each neuron. HVC_{RA} neurons burst at a single precise time during the song.

The activity patterns are shown on a shorter time scale in Fig. 16. The firing behavior of a sample class B interneuron (HVC^2_{INTB}) is shown in Fig. 16 along with firing of HVC^2_{INTA} and HVC^2_{RA}. In this network, HVC^2_{INTB} (black trace) is continuously spiking until HVC^2_{INTA} (red trace) elicits a burst of activity inhibiting it. This inhibition allows HVC^2_{RA} (blue trace) to escape and fire a burst of activity.

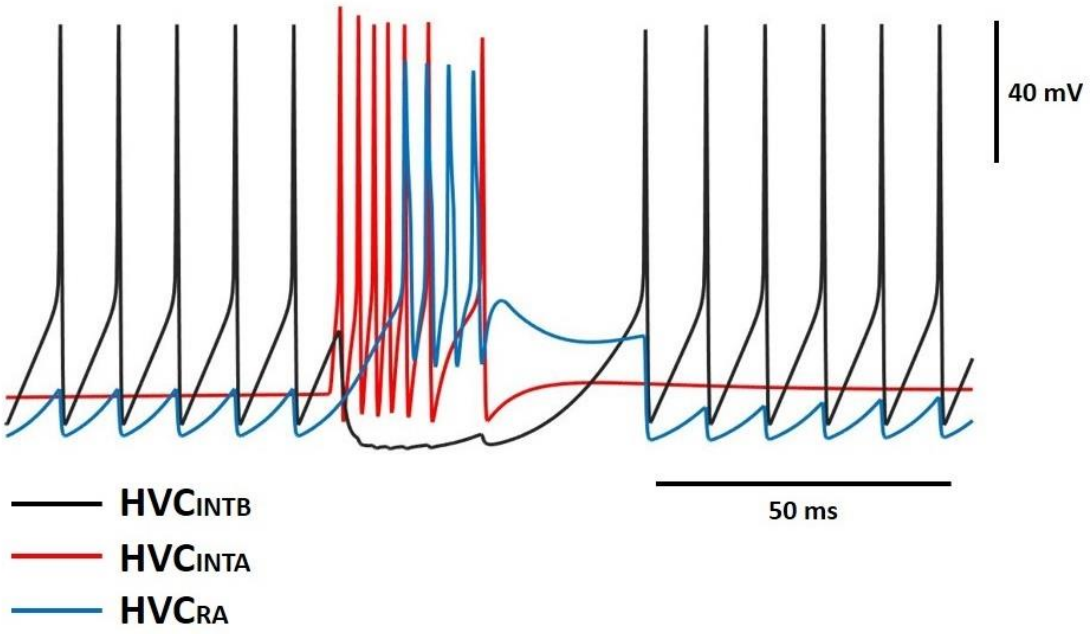

Figure 16: Zoomed version of HVC spiking patterns of network architecture two: The burst in HVC_{INTA} (red) inhibits HVC_{INTB} (black) which allows HVC_{RA} (blue) to escape inhibit and fire a burst of activity.

Although this network produces the desired behavior of HVC neurons, one possible drawback is that class A interneurons fire only one burst in response to excitation from HVC_{RA} bursts. Recordings of identified HVC neurons in singing birds have shown that HVC_{INT} neurons can fire up 5-10 bursts per song motif (Hahnloser *et al.*, 2003; Leonardo &

Fee, 2005; Hahnloser *et al.*, 2006). Another possible drawback is that the sequence of activity in HVC_{RA} neurons is driven primarily by the lack of excitation in HVC_{INTB} neurons due to HVC_{INTA} inhibition. While some studies have shown an important role for HVC_{INT} – HVC_{INT} interactions in the production of the song and the bird's recognition of its own song (Kubota & Taniguchi, 1998; Mooney, 2000; Hahnloser *et al.*, 2003; Rosen & Mooney, 2003), other studies showed that they don't play a role (Scharff *et al.*, 2000; Long *et al.*, 2010). These factors also motivate the investigation of additional networks.

5.3. Network 3: Recruitment of all classes of HVC neurons

The third network architecture, displayed in Fig. 17, incorporates the three HVC neuronal classes into the dynamics. We envisioned the HVC network as comprised of several microcircuits where each microcircuit contains neurons from all classes of HVC neurons. Each microcircuit has its own internal dynamics which then sends its output to the next microcircuit in the chain. Within each of the microcircuits (the first of which is enclosed by a dashed rectangle), there are excitatory projections from HVC_{RA} back onto HVC_{RA} and from HVC_{RA} to HVC_{INT} and inhibitory projections from HVC_{INT} to HVC_{X}. The microcircuits interact with each other via the projections from HVC_{X} from one microcircuit to HVC_{RA} in a following microcircuit.

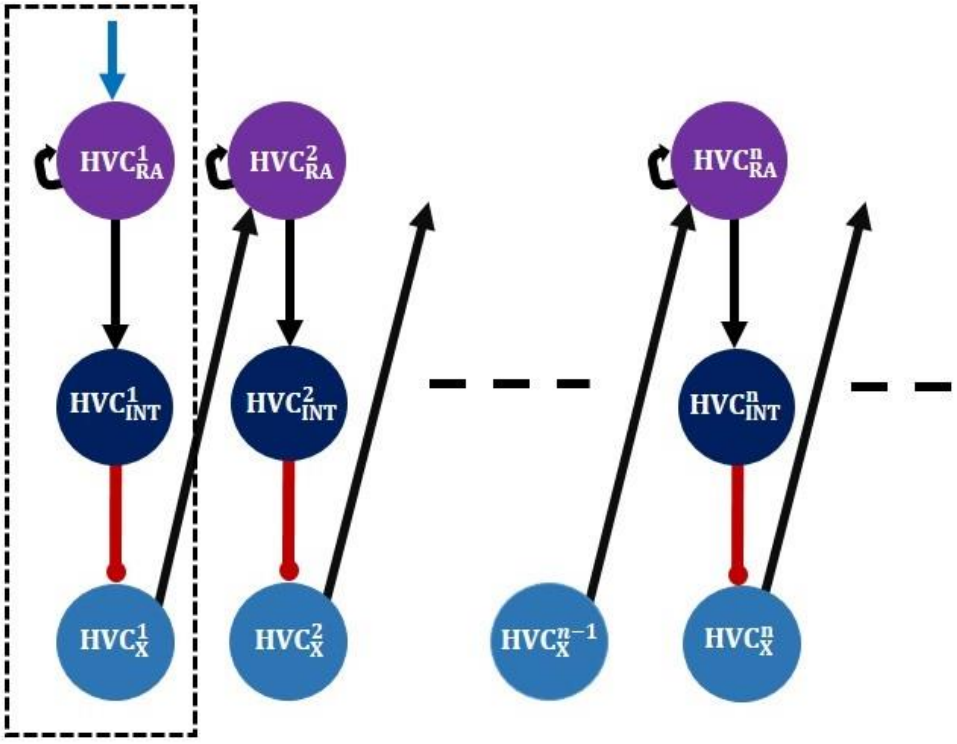

Figure 17: Arrangement of prototype network architecture three. Black arrows symbolize excitation via AMPA currents. Red arrows (with circle heads) symbolize inhibition via GABA currents. The blue arrow symbolizes DC input. The first microcircuit is enclosed by a dashed rectangle to represent its role as a leading microcircuit in the network.

In every microcircuit, each HVC^{i}_{RA} neuron excites an HVC^{i}_{INT} neuron via AMPA/NMDA currents; HVC^{i}_{INT} neuron in its turn inhibits HVC^{i}_{X} via GABA currents. Each HVC^{i}_{X} in microcircuit (*i*) excites HVC^{i+1}_{RA} in the next microcircuit (*i+1*) via AMPA/NMDA currents to ensure propagation of the pulse through the subsequent microcircuit. The first HVC_{RA} neuron receives an excitatory drive (DC input) from outside the HVC (blue arrows in diagram) to quick start the network.

The activity patterns that this network displays are shown in Fig. 18. HVC_{RA} neurons bursting requires AMPA/NMDA excitation from each HVC^{i}_{RA} to itself. When

HVC_{RA}^{1} receives the driving input, it elicits a burst of several spikes (Fig. 18A). This firing induces HVC_{INT}^{1} bursting due to AMPA excitatory coupling (Fig. 18B). Now, HVC_{X}^{1} , that was inhibited by HVC_{INT}^{1} due to GABA inhibitory coupling, generates a rebound burst of activity once the inhibiting input is removed (Fig. 18C). The spiking in HVC_{RA}^{1} is amplified by the excitatory projection back onto HVC_{RA}^{1}. HVC_{X}^{1} in its turn generate a burst in HVC_{RA}^{2} in the second microcircuit due to excitatory AMPA coupling. In particular, HVC_{X}^{1} generates a burst of activity in HVC_{RA}^{2} due to strong excitatory AMPA drives, which then in its turn carries the chain of activity across HVC_{INT}^{2} and HVC_{X}^{2} in a similar fashion to the first microcircuit. This activity propagates throughout the chain of microcircuits causing a sequence of HVC_{X}, HVC_{INT} and HVC_{RA} bursts (Fig. 18).

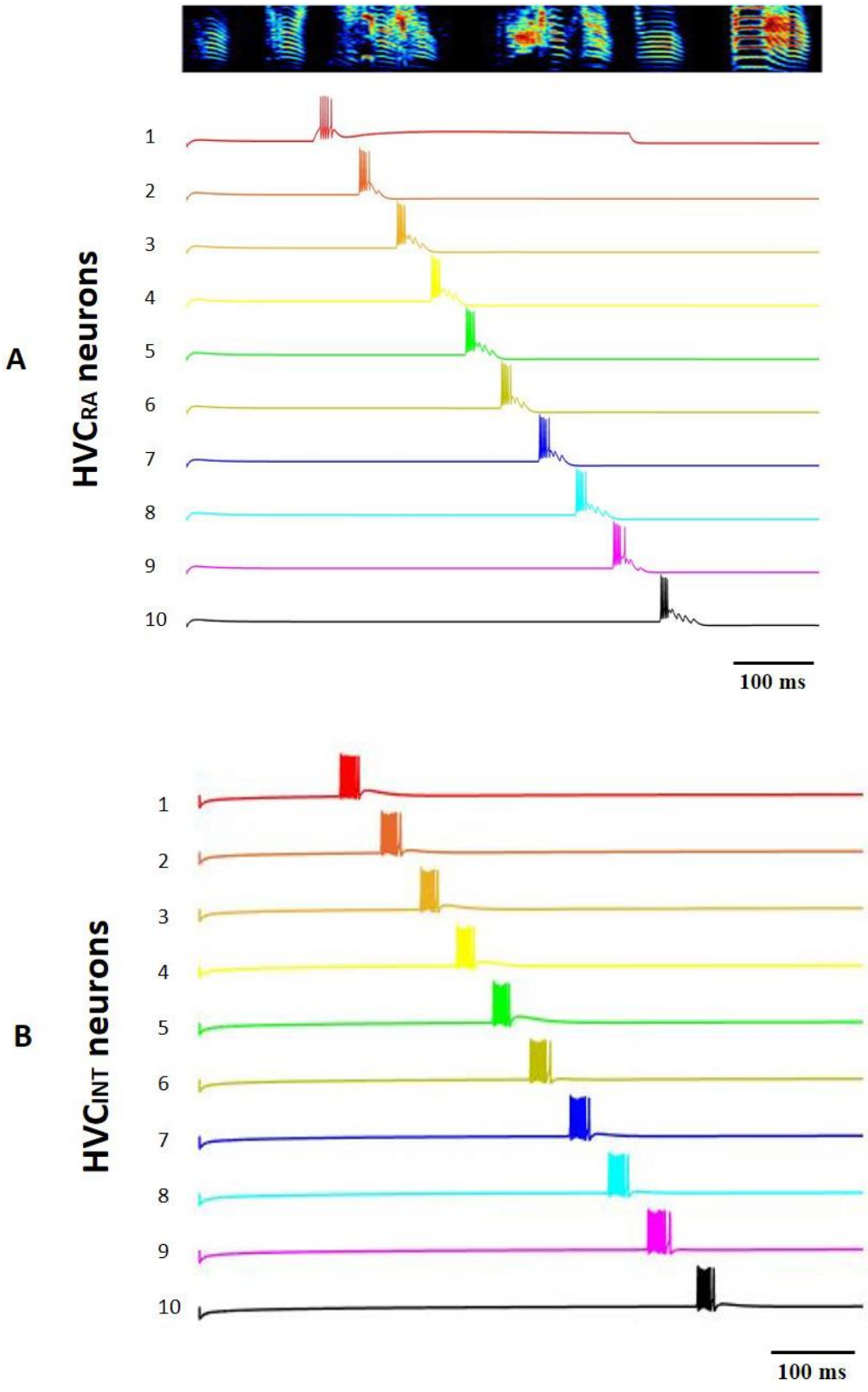
A
HVCRA neurons
1
2
3
4
5
6
7
8
9
10
100 ms
B
HVCINT neurons
1
2
3
4
5
6
7
8
9
10
100 ms

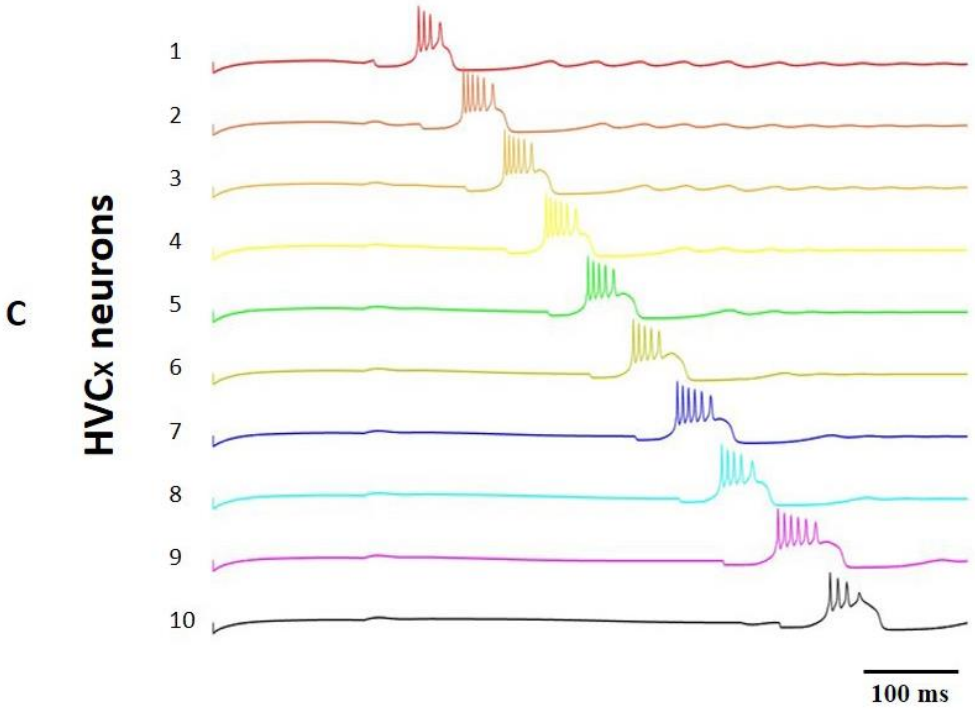

Figure 18: HVC spiking patterns of network architecture three. All three classes of HVC neurons show a sequential propagation of bursts throughout the network.

The effects of excitatory coupling between HVC_{RA} and HVC_{INT}, the inhibitory coupling between HVC_{INT} and HVC_X as well as the rebound bursting in HVC_X are all illustrated in Fig.19. In this figure, the firing patterns of neurons from microcircuit two are shown. When HVC_{RA}^2 (green trace, Fig. 19A-B) generates its burst of activity (due to excitatory synaptic drive from HVC_{RA}^2 onto itself), a burst of activity is generated in HVC_{INT}^2 (red trace, Fig. 19A-B) at the same time due to fast AMPA currents. This burst in HVC_{INT}^2 inhibits HVC_X^2 (black trace, Fig. 19A-B) due to GABA coupling (notice the sag due to inhibition in HVC_X^2 at the same onset in time HVC_{INT}^2 generates its burst, Fig. 19B). When HVC_{INT}^2 finishes its burst, HVC_X^2 is able to escape the inhibition and fires a post-inhibitory rebound burst due to the T-type Ca^{2+} (I_{CaT}) and the hyperpolarization activated inward (I_h)

currents it exhibits. This burst in HVC_X^2 is the key factor that transmits the activity to the next microcircuit via HVC_X^2 - HVC_{RA}^3 excitatory coupling.

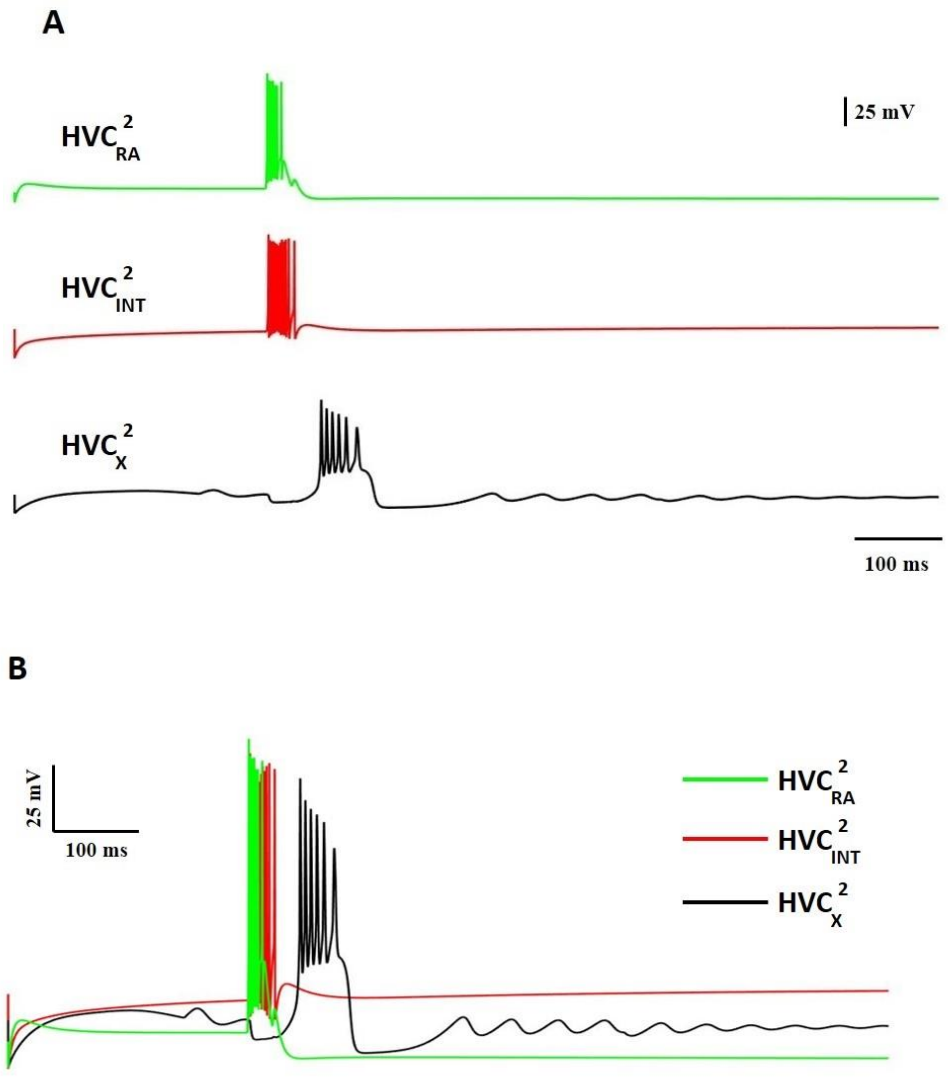

Figure 19: The patterns of the classes of HVC neurons in a sample microcircuit of Network 3, here microcircuit two: A. The burst in HVC_{RA}^2 (green) induces a burst in HVC_{INT}^2 (red) due to excitatory NMDA/AMPA coupling. HVC_{INT}^2 bursting elicits a strong inhibition in HVC_X^2 (black) due to GABA coupling, which then escapes the inhibition and fires a post-inhibitory rebound burst of activity. B. The same traces in panel A overlaid.

As in the previous networks, the strength of the HVC_{RA} bursts are dependent on the strength of the excitatory synapse from HVC_{RA} onto itself as well as the speed of Ca^{2+}-build up that activates the SK-current which plays the role in truncating the burst. Furthermore, tuning of g_{KNa} conductance was necessary to limit the bursting to one burst per neuron underlining the role of I_{KNa} in damping the excitability of HVC_{RA} neurons. The strength and duration of the HVC_{INT} burst is solely dependent on the strength of the excitatory synaptic conductance from HVC_{RA} onto HVC_{INT}. Interneurons do not exhibit ligand-gated inhibitory conductances (I_{SK} or I_{KNa}) like the other two classes of HVC neurons and are known to be very fast spikers; therefore, the only factor in this network that determines the strength and duration of HVC_{INT} bursts are the synaptic conductances that couple them with their efferent inputs. And finally, the strength and the location of the HVC_X post-inhibitory rebound burst is determined by two factors: 1- The degree of inhibition from HVC_{INT} onto HVC_X characterized by the GABA conductances, and 2- The magnitudes of the T-type Ca^{2+}- and the H- conductances that work cooperatively to generate extra and strong excitatory drives when the neuron escape inhibition (Daou et al. 2013). Not to mention that the I_{SK} current plays a key role in damping the excitability of HVC_X neurons. For smaller g_{SK} conductances, higher number of bursts is observed in HVC_X neurons. We also noticed that the increase in I_{CaT} magnitude induces a depolarization plateau that hinder the neuron from returning to the resting membrane potential. In order to surpass this problem, tuning of the g_{CaT} and g_K conductances was necessary.

This network was designed with the aim to incorporate for the first time the three classes of HVC neurons in one network architecture. The ionic currents magnitudes and the synaptic strengths were calibrated to propagate sequential activity, but one of the drawbacks of this network is that both HVC interneurons and HVC_X neurons generate a single burst throughout the song with HVC interneurons not firing sparsely as they are known to do *in vivo*. We can connect multiple HVC_{RA} neurons onto a single HVC_{INT} neuron, and hence each time any of the connected HVC_{RA} neurons bursts, it'll generate a burst in the interneuron thereby collectively creating multiple bursts in that HVC_{INT} neuron at different times. The problem with this scenario is that multiple bursts in a single HVC_{INT} will create equal number of post-inhibitory rebound bursts in the corresponding HVC_X neuron in the same microcircuit. This is a problem because the sequential activity propagates to the subsequent microcircuits via HVC_X-HVC_{RA} connectivity, and multiple bursts in an HVC_X will create multiple bursts in the HVC_{RA} neuron its connected too, which will 1) break down the sequence propagation and 2) not realistic biologically as HVC_{RA} neurons fire a single burst during singing. These factors will be addressed in the next network architecture. However, to address the sparse firing of HVC_{INT} neurons, we injected to our model interneurons a stochastic input current instead of constant DC pulse with the aim to make these neurons spike densely throughout the song.

The activity patterns that the stochastic version of this network incorporates are shown in Fig 20. Sequential bursts propagation have been replicated similarly in the three classes of neurons like described earlier (Fig. 19). In particular, HVC_{RA} neurons (Fig. 20A) elicit single bursts at one instance of time during the song. These bursts generate strong bursts of action potentials in the HVC_{INT} neurons (Fig. 20B) of the same microcircuit,

which then trigger a post-inhibitory rebound bursts in HVC_X neurons (Fig. 20C) The main difference here is the sparse firing that HVC interneurons now exhibit (Fig. 20B) which was not the case earlier (Fig, 18B). This makes the firing of this class of neurons more biologically realistic. However, tuning of the model parameters was necessary to conserve the sequential propagation especially in HVC_X neurons that are able to rebound burst after a series of weak inhibitory synaptic inputs coming from interneurons and not only as a result of a strong interneuron burst inhibiting HVC_X. For example, notice the sag (inhibition) each HVC_X^i neuron exhibit when a spike is elicited by HVC_{INT}^i in the same microcircuit (Fig. 20C). This small inhibition in HVC_X^i is able to generate a rebound spike or burst in the neuron; however, with the tuning that was applied, we were able to generate a rebound burst only when HVC_{INT}^i neuron generates its single burst. The success of this model manipulation is a strong indicator of the robustness of the model that is able to generate almost the same behavior in the presence of some random inputs.

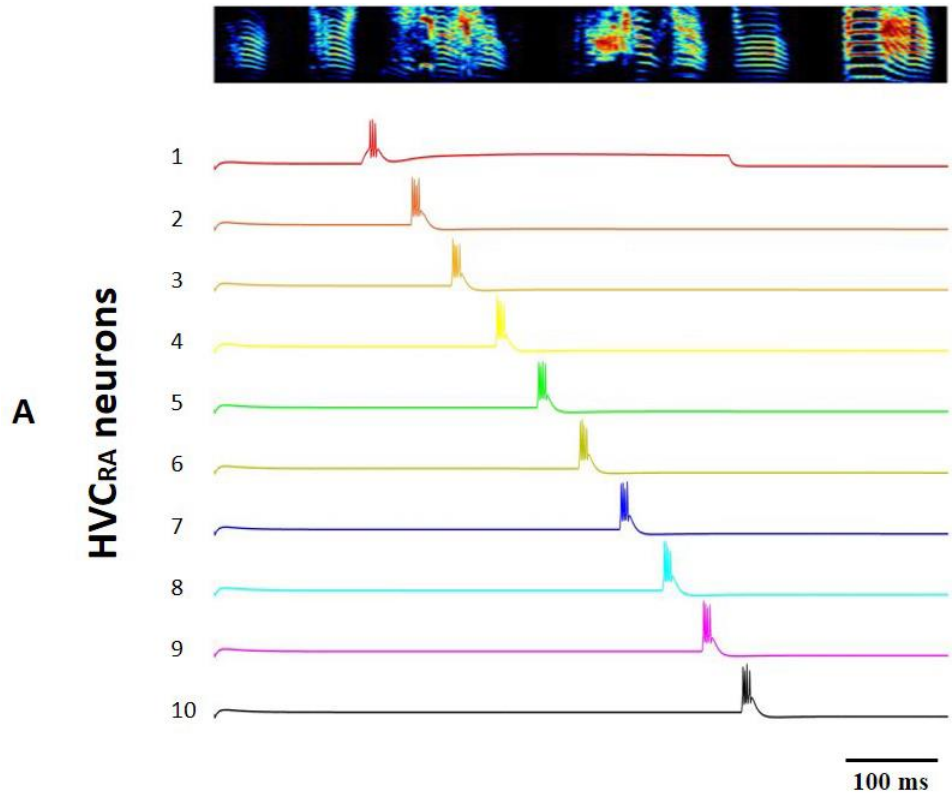
A
HVCRA neurons
1
2
3
4
5
6
7
8
9
10
100 ms

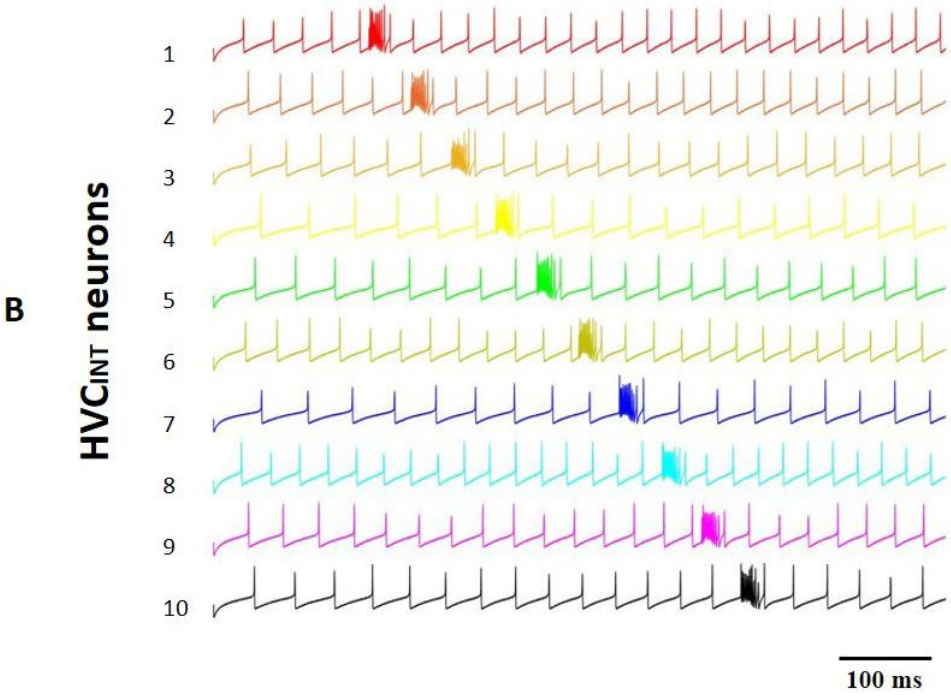
B
HVCINT neurons
1
2
3
4
5
6
7
8
9
10
100 ms

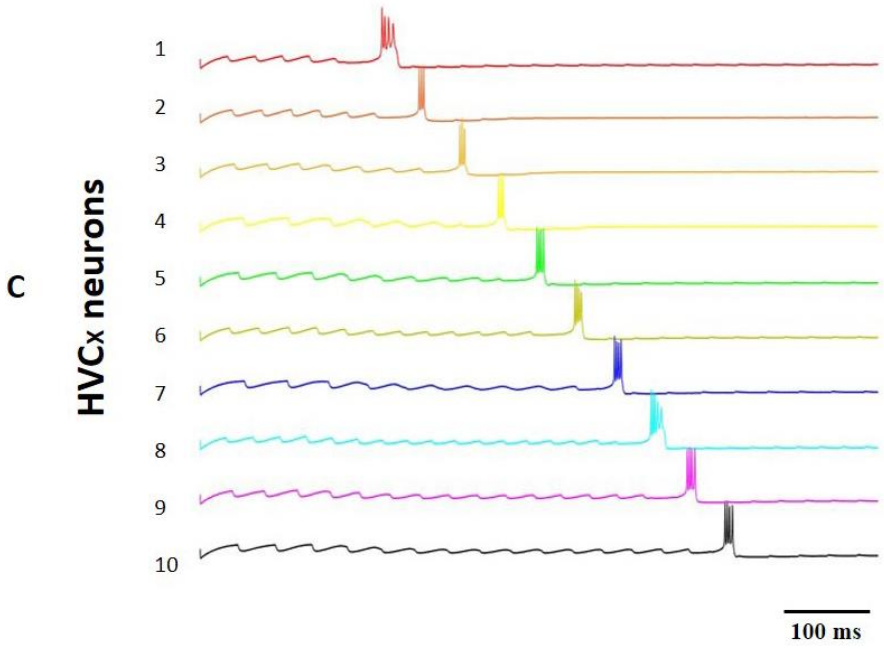

Figure 20: HVC spiking patterns of network architecture three while incorporating a stochastic input to HVC interneurons. All three classes of HVC neurons show a sequential propagation of bursts throughout the network as shown previously (Fig. 18) with the exception that this time HVC_{INT} neurons fire sparsely throughout the song.

5.4. Network 4: Towards an *in vivo* realistic network

The fourth architecture, displayed in Fig. 21, gives more complex and biologically realistic network dynamics than the previous networks as it incorporates all classes of HVC neurons similar to network three as well as replicate the firing patterns with more accuracy. Each microcircuit here is comprised of a random number of HVC_{RA} neurons (to be described below) in addition to an interneuron and an X-projecting neuron. In this chain model, burst timing and propagation is controlled by a synaptic input from a preceding group of HVC_{RA} neurons connected via AMPA currents. In other words, all of HVC_{RA} neurons were connected in a synfire chain mode (similar to network one in this aspect). Each of N (= 55 in our simulation, but it could be any number) HVC_{RA} neurons could

belong to one or more microcircuits, chosen randomly to belong to this microcircuit or the other. Each HVC_{INT} in a microcircuit was assigned a random number of connections from HVC_{RA} neurons (3 to 6 HVC_{RA} neurons). Therefore, the number of HVC_{RA} neurons to connect to the interneuron is random, as well as which HVC_{RA} neurons are to synapse onto the interneuron was also random. Each HVC_{INT} neuron in its turn inhibit a single HVC_X neuron. The stable propagation of bursts requires fine tuning of synaptic strengths to avoid runaway excitation or decay.

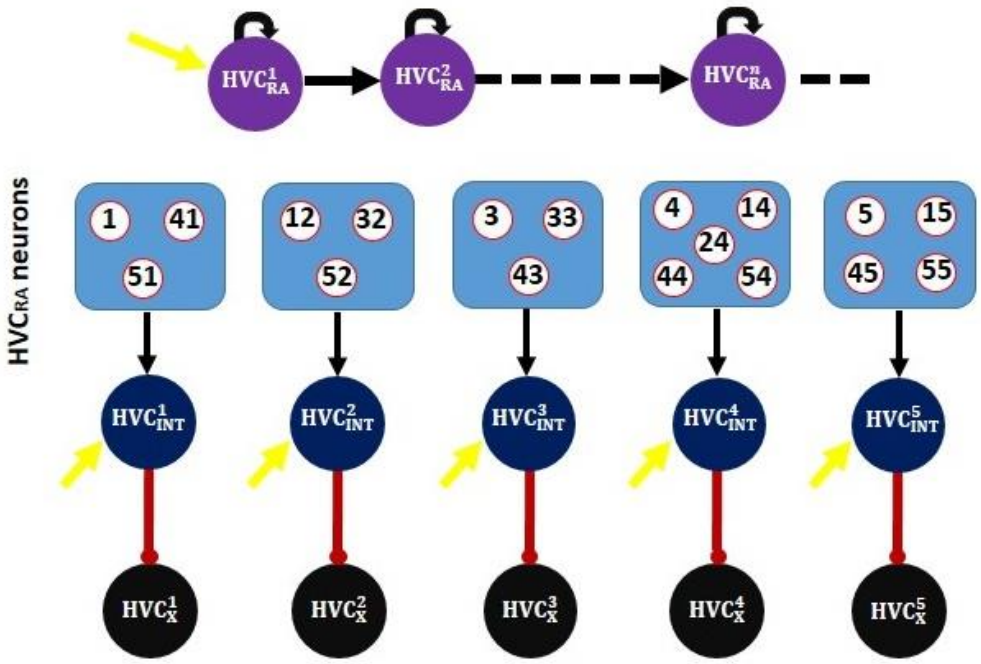

Figure 21: Arrangement of prototype network architecture four. Black arrows symbolize excitation via AMPA currents. Red arrows (with circle heads) symbolize inhibition via GABA currents. The yellow arrows symbolize DC inputs. Each blue box entails the number of HVC_{RA} neurons that were recruited randomly to inhibit an HVC interneuron.

The activity patterns that this network displays are shown in Fig. 22. Only HVC_{RA}^{1} neuron receives a DC pulse to kick start the network. The chain of bursts in HVC_{RA} neurons was reproduced in a similar fashion as in Network 1 (Fig. 22A). Similar to the observed *in vivo* behavior, and due to the several connections they receive from the various HVC_{RA} neurons randomly, HVC interneurons generate multiple bursts throughout the song (Fig. 22B) which is what's seen in singing birds. Finally, HVC_{X} model neurons fire between 1 and 3 bursts throughout song similar to the experimental results (Hahnloser *et al.*, 2003). Furthermore, HVC_{X} neurons differed in the number of bursts and the number of spikes per burst making the results more realistic.

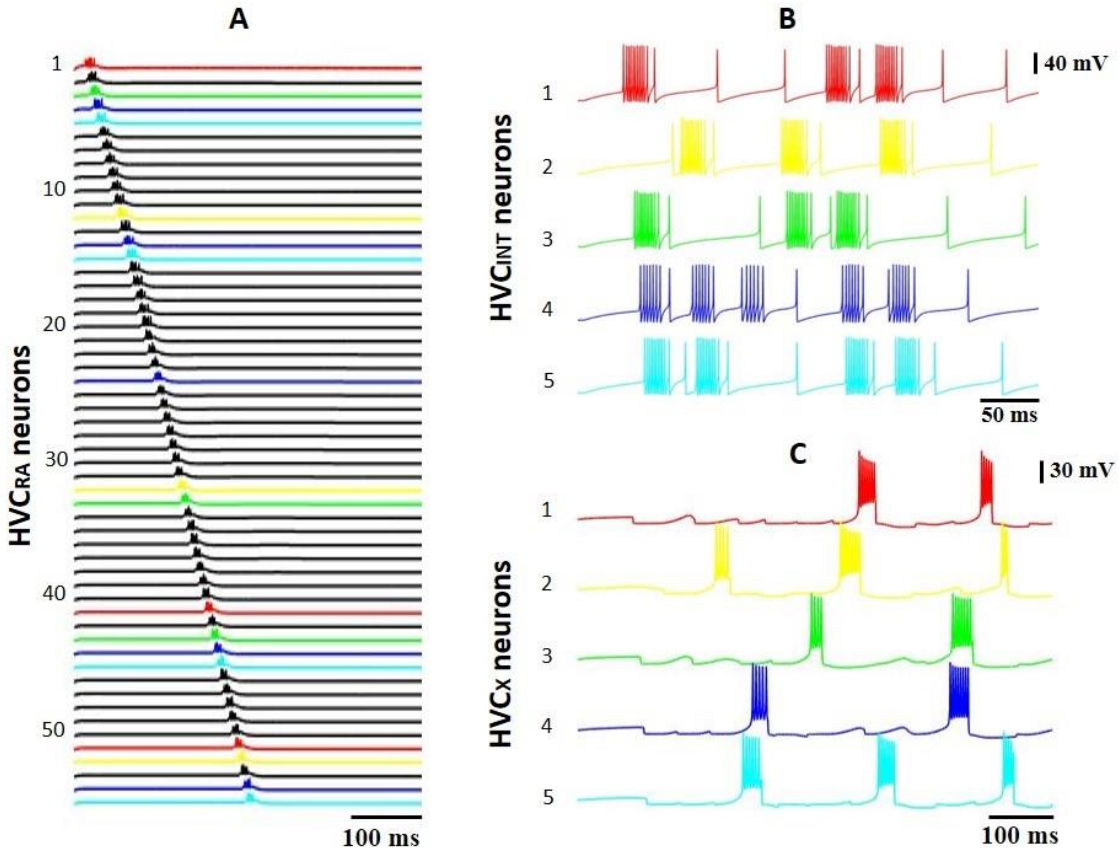

Figure 22: HVC neurons spiking patterns of network architecture four. A: Sequential bursting of HVC_{RA} neurons within the network. B: HVC interneurons activity displays dense spiking throughout the song while eliciting multiple bursts of activity at different times. C: HVC_X neurons bursting activity throughout the song shows multiple bursts unlike networks 1-3.

The random connections from HVC_{RA} neurons to HVC_{INT} as well as the multiple bursts HVC_{INT} and HVC_X exhibit in this network are illustrated in Fig. 23. Here the firing pattern for HVC_{INT}^{5} is shown (black trace) along with the 4 HVC_{RA} neurons (blue traces) that were chosen randomly to send their synpases onto the interneuron. Notice that each HVC_{RA} neuron bursts only once as reported experimentally (Hahnloser *et al.*, 2003). The time difference between the bursts of the 4 HVC_{RA} neurons is due to the fact that there are

multiple other HVC_{RA} neurons that burst in between in the chain of HVC_{RA} neurons, but that are not shown here (only those that connect onto HVC_{INT}^{5} are shown). HVC_{INT}^{5} neuron generate here 4 bursts within the song as well as spike sparsely, as reported experimentally as well (Hahnloser *et al.*, 2003). Each of the 4 bursts in HVC_{INT}^{5} is aligned with one of 4 bursts in HVC_{RA} neurons (blue traces) due to excitatory coupling. And finally, HVC_{X}^{5} neuron generates multiple postinhibitory rebound bursts due to the inhibitory coupling with HVC_{INT}^{5}. The number of bursts in HVC_{X} neurons need not be necessarily the same number of bursts in its associated HVC_{INT} neurons (for example in this case HVC_{X}^{5} exhibit 3 bursts while HVC_{INT}^{5} exhibits 4 bursts), because if the HVC_{INT} neuron generated multiple successive bursts of firing, HVC_{X} neuron can not escape inhibition within the short time interval between bursts (Fig. 23), and need more time until the time interval between bursts is long enough for the I_h and I_{CaT} currents to fully activate and generate a reboud burst. This all makes the firing of these three classes of neurons more realistic and adheres with the reported literature.

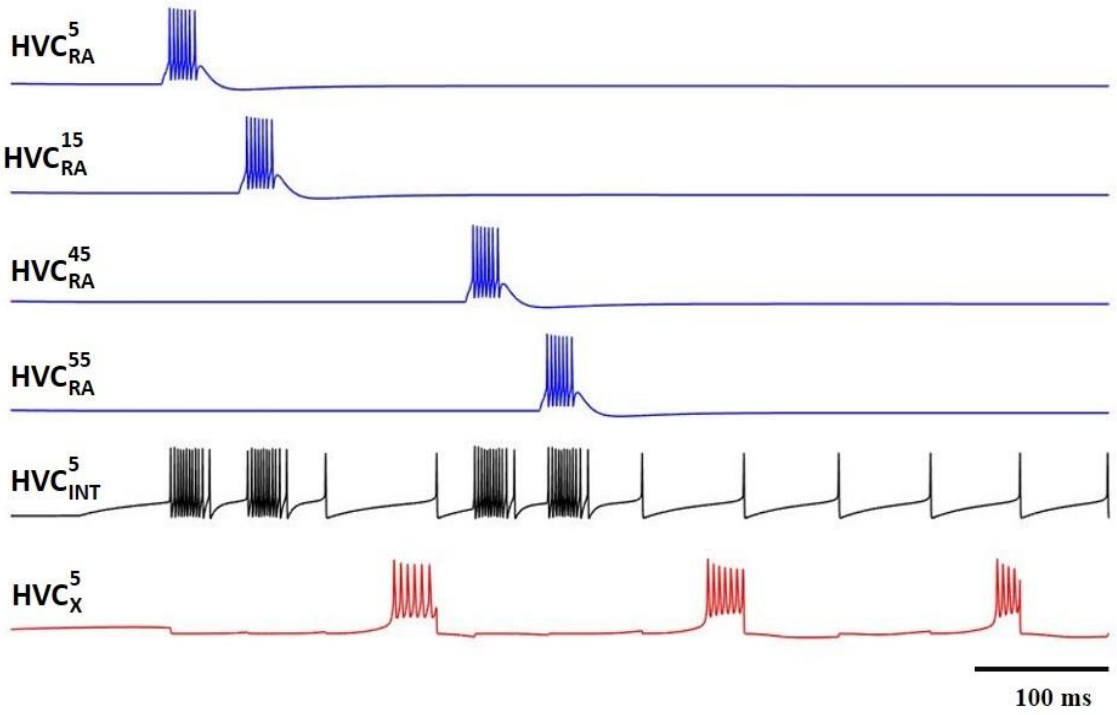

Figure 23: HVC_X^5, HVC_{INT}^5 and their associated HVC_{RA} neurons spiking patterns. Sequential bursting of HVC_{RA} neurons induces sparse bursting in HVC interneurons resulting in multiple bursts of activity in HVC_X neurons.

Our simulations in this network chooses randomly the inputs from HVC_{RA} to HVC_{INT} neurons to reflect the biological reality that 1) we don't know which of the HVC_{RA} neurons connect to the interneuron and 2) to show that no matter which HVC_{RA} neurons connect to the interneuron, the sequential propagation of activity is not altered and the firing patterns of the interneuron and the X-projecting neurons remains biologically realistic. However, in a biological network once the connections are made from one neuron to another, this synapse does not change its afferent input to another neuron during each rendition of behavior (like song in our case), and the number of connections into and from the neuron remains largely unaltered over short periods of time. Therefore, to simulate this

mechanism, for the same set of random inputs from HVC_{RA} neurons onto HVC_{INT} neurons, we observe that HVC_X neurons exhibit time-locked firing patterns to vocalizations (Fig. 24) that remains unaltered even though the model network starts from different initial conditions. These results had been shown before for HVC_X neurons in singing birds (Fujimoto *et al.*, 2011).

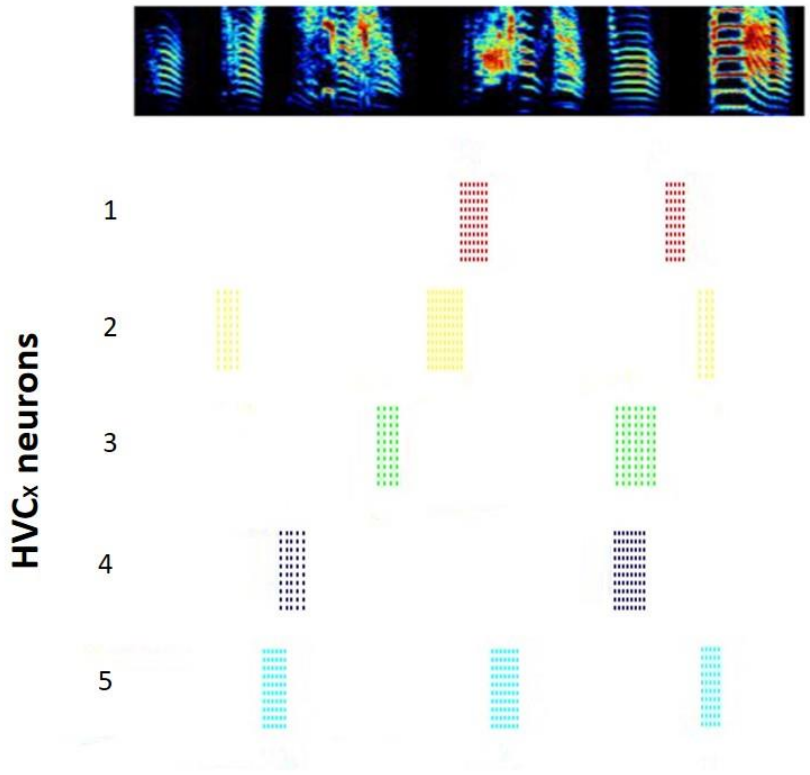

Figure 24: Spike raster plot of HVC_X neurons showing the time locked firing of neurons relative to vocalizations. Each row of tick marks shows spikes generated during one rendition of the song or call, modeled as starting the simulation from different initial conditions; roughly ten renditions are shown for each neuron.

Finally, to make our model even more realistic, we injected each of our model HVC_X and HVC_{INT} neurons with stochastic input currents, representing the ascending auditory inputs these neurons receive, because it's certainly unrealistic that biological neurons receive DC-like inputs.

The activity patterns that the stochastic version of this network incorporates are shown in Fig 25. Sequential bursts propagation have been replicated similarly in HVC_{RA} neurons like described earlier (Fig. 22). In particular, HVC_{RA} neurons (Fig. 25A) elicit single bursts at one instance of time during the song. These bursts generate strong bursts of activity in the associated HVC interneurons (Fig. 25B), which then trigger a post-inhibitory rebound bursts in HVC_X neurons (Fig. 25C). The main difference here is the sparse firing that HVC interneurons now exhibit (Fig. 25B) that is a result of a stochastic input applied to these neurons instead of a DC pulse. This makes the firing of this class of neurons more biologically realistic. However, delicate tuning of the model parameters was necessary to ensure a number of bursts in HVC_X neurons limited to 1-3 bursts. Replicating the HVC_X neurons firing pattern remains the most challenging part of the network since this class of neurons is able to rebound burst after a series of weak inhibitory synaptic inputs coming from interneurons and not only as a result of a strong interneuron burst inhibiting HVC_X. The challenge here was to smartly tune the network parameters to be able to regenerate the *in vivo* behavior of the three classes of neurons while applying a stochastic input that varies from one simulation to the other. Here, the stochastic inputs ranges was chosen in a way to generate the desired pattern of activity in the three classes of HVC neurons while adding a more realistic component to the network and this is what makes the robustness of this model.

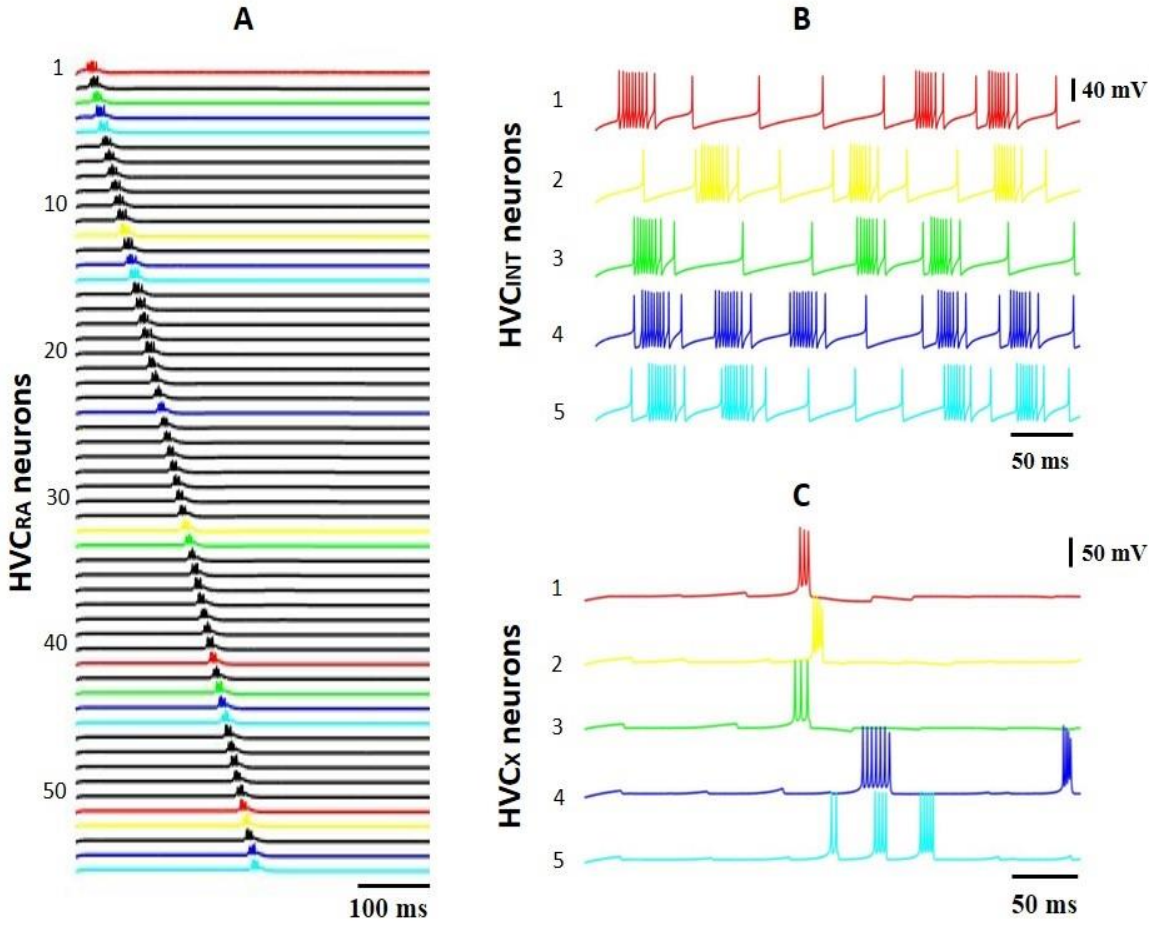

Figure 25: HVC spiking patterns of network architecture four. A stochastic input was incorporated to HVC interneurons and HVC_X neurons while quick starting the network with a random DC input applied to HVC_{RA}^{1} . A: HVC_{RA} neurons show a sequential propagation of bursts throughout the network. B: HVC_{INT} neurons fire sparsely throughout the song while exhibiting several bursts of activity. C: HVC_X neurons fire different number of bursts (1-3 bursts) similar to experimental results.

By far, this is the best network architecture that we generated that's able to replicate with high accuracy the firing patterns of the three classes of HVC neurons *in vivo*. In other words, it's able to 1) generate the temporally precise time-locked 5-10 ms bursts of HVC_{RA} neurons and in a sequential syn-fire chain mode that's seen *in vivo* (Hahnloser *et al.*, 2003; Long *et al.*, 2010), 2) generate the sparse bursting and spiking in HVC interneurons (Hahnloser *et al.*, 2003), and 3) generate the time-locked and multiple bursts of HVC_X neurons (Fujimoto *et al.*, 2011) .

CHAPTER 6

CONCLUSION

We have presented computational models that describe how sequential activity in HVC projection neurons can be produced during singing. These microcircuit chains are envisioned to have many copies throughout the HVC, and the chain ensemble is envisioned to drive singing. The fitting and calibration of the HVC neurons architectures succeeded in regenerating the *in vivo* firing patterns of the three classes of HVC neurons, in particular, the sequential propagation of bursts in the HVC_{RA} population, the sparse bursting of HVC_X neurons and the high frequency bursting with dense spiking of HVC interneurons. The patterning activity in HVC is shaped by synaptic inputs and the interplay between excitation and inhibition, which enables HVC_{RA}, HVC_X and HVC_{INT} neurons to generate their characteristic bursts during singing. At the network level, each neuron's behavior affects the overall communication inside the neural network which makes biological neural networks one of the most challenging and complex systems to understand and replicate computationally.

The different chain architectures that we described produce different activity patterns of HVC neurons, and lead to different predictions. For example, inhibitory projections are crucial for the sequential activity in the last three architectures, so antagonism of GABA receptors would terminate the activity pattern. The last three architectures predict a key role for post-inhibitory rebound of HVC_X neurons. The different networks also predict a different number of bursts per motif of HVC_{INT} and of HVC_X

neurons. At present, there are insufficient data to determine which of the proposed architectures are best representative of the HVC circuitry. However, the model networks provide insight into how the different types of HVC neurons can be used for sequence generation.

Chain models have previously been proposed for the HVC (Li & Greenside, 2006; Jin *et al.*, 2007; Long *et al.*, 2010). Although the HVC neurons in our model are segregated into a chain-like network of microcircuits, we have focused on the interactions among the three classes of HVC neurons. Unlike other models, our simulations and analysis propose that post-inhibitory rebound in most networks, particularly networks two through four, plays a key role in preserving precise timing information that enables reliable propagation of sequential activity throughout the HVC microcircuits. This mechanism is a characteristic of some invertebrate central pattern generators which use inhibition and recurrent excitation and which exhibit post-inhibitory rebound (Satterlie, 1985; Goaillard *et al.*, 2010).

Although our model includes chainlike networks, we have focused on the role of inhibition and rebound firing rather than chains. Unlike other chainlike models, our model postulates a central role for inhibitory interneurons and X-projecting neurons in sparsely bursting telencephalic premotor networks, HVC in particular. This mechanism is related to those of central pattern generators and cortical networks, which make use of inhibition and recurrent excitation (McCormick 2005; Shu *et al.*, 2003; Yuste *et al.*, 2005).

The various networks that we have examined raise developmental questions. What developmental mechanism could generate the pattern of HVCINT → HVCRA connectivity in networks two, three and four? Little is known about the development of the inhibitory inputs from interneurons onto the projection neurons within the HVC. However, we suggest

a mechanism whereby the excitatory coupling between the projection neurons and the interneurons develops early in the bird's life and interneuron connectivity develops later as the bird attempts to reproduce the song of its tutor. Thus, the interneurons inhibit specific projection neurons to move the brain circuitry in a direction that minimizes the error in vocal output relative to that of the tutor's song. Moreover, this study of the architecture of the HVC nucleus is able to give us insights of the physiological changes taking place inside the bird's brain while vocalizing. Our model will bring songbird research a step closer to understanding the network connectivity behind the spatio-temporal sequences generated by HVC neurons. Understanding how the HVC circuitry operates to generate this sequential propagation is a stepping stone towards deciphering how neural networks in the human brain communicate to execute complex motor skills that require as well prior planning into proper spatial and temporal ordered sequences.

In closing, the work presented in this dissertation has the potential to make a considerable impact in the field of songbird research. The computational models developed provide a large step forward in describing the biophysics of HVC neurons. This work serves as step towards discussing realistic and plausible neural architectures that would reflect an accurate topography of the nucleus as well as produce the characteristic patterns of neural activity exhibited by the various HVC neurons during singing. Being able to explain the complete story of the neural code behind HVC's sequential activity could open a new era to science.

REFERENCES

Abarbanel, H.D., Gibb, L., Mindlin, G.B., Rabinovich, M.I. & Talathi, S. (2004a) Spike timing and synaptic plasticity in the premotor pathway of birdsong. *Biological cybernetics*, **91**, 159-167.

Abarbanel, H.D., Talathi, S.S., Mindlin, G., Rabinovich, M. & Gibb, L. (2004b) Dynamical model of birdsong maintenance and control. *Physical Review E*, **70**, 051911.

Abeles, M. (1991) *Corticonics: Neural circuits of the cerebral cortex*. Cambridge University Press.

Ahmed, S., de Jager, C.A., Haigh, A.-M.F. & Garrard, P. (2012) Logopenic aphasia in Alzheimer's disease: clinical variant or clinical feature? *J Neurol Neurosurg Psychiatry*, **83**, 1056-1062.

Albert, C.Y. & Margoliash, D. (1996) Temporal hierarchical control of singing in birds. *Science*, **273**, 1871-1875.

Amari, S.-I. (1972) Learning patterns and pattern sequences by self-organizing nets of threshold elements. *IEEE Transactions on Computers*, **100**, 1197-1206.

Armstrong, E. (2018) Computational model of avian nervous system nuclei governing learned song. *arXiv preprint arXiv:1801.06226*.

Armstrong, E. & Abarbanel, H.D. (2016) Model of the songbird nucleus HVC as a network of central pattern generators. *Journal of neurophysiology*, **116**, 2405-2419.

Bolhuis, J.J. & Gahr, M. (2006) Neural mechanisms of birdsong memory. *Nature reviews neuroscience*, **7**, 347-357.

Bolhuis, J.J., Gobes, S.M., Terpstra, N.J., den Boer-Visser, A.M. & Zandbergen, M.A. (2012) Learning-related neuronal activation in the zebra finch song system nucleus HVC in response to the bird's own song. *PLoS One*, **7**.

Bolhuis, J.J., Okanoya, K. & Scharff, C. (2010) Twitter evolution: converging mechanisms in birdsong and human speech. *Nature Reviews Neuroscience*, **11**, 747-759.

Booth, J.R., Wood, L., Lu, D., Houk, J.C. & Bitan, T. (2007) The role of the basal ganglia and cerebellum in language processing. *Brain research*, **1133**, 136-144.

Bragoni, M., Altieri, M., Di Piero, V., Padovani, A., Mostardini, C. & Lenzi, G. (2000) Bromocriptine and speech therapy in non-fluent chronic aphasia after stroke. *Neurological Sciences*, **21**, 19-22.

Brainard, M.S. & Doupe, A.J. (2000) Auditory feedback in learning and maintenance of vocal behaviour. *Nature Reviews Neuroscience*, **1**, 31.

Brenowitz, E.A., Margoliash, D. & Nordeen, K.W. (1997) An introduction to birdsong and the avian song system. *Journal of neurobiology*, **33**, 495-500.

Cannon, J., Kopell, N., Gardner, T. & Markowitz, J. (2015) Neural sequence generation using spatiotemporal patterns of inhibition. *PLoS Comput Biol*, **11**, e1004581.

Chew, S.J., Vicario, D.S. & Nottebohm, F. (1996) A large-capacity memory system that recognizes the calls and songs of individual birds. *Proceedings of the National Academy of Sciences*, **93**, 1950-1955.

Daou, A. & Margoliash, D. (2020) Intrinsic neuronal properties represent song and error in zebra finch vocal learning. *Nature communications*, **11**, 1-17.

Daou, A., Ross, M.T., Johnson, F., Hyson, R.L. & Bertram, R. (2013) Electrophysiological characterization and computational models of HVC neurons in the zebra finch. *Journal of neurophysiology*, **110**, 1227-1245.

Day, N.F., Kinnischtzke, A.K., Adam, M. & Nick, T.A. (2009) Daily and developmental modulation of "premotor" activity in the birdsong system. *Developmental neurobiology*, **69**, 796-810.

DestexheCA, A. & Babloyantz, A. (1993) A model of the inward current Ih and its possible role in thalamocortical oscillations. *Neuroreport*, **4**, 223-226.

Doupe, A.J. & Kuhl, P.K. (1999) Birdsong and human speech: common themes and mechanisms. *Annual review of neuroscience*, **22**, 567-631.

Drew, P.J. & Abbott, L. (2003) Model of song selectivity and sequence generation in area HVc of the songbird. *Journal of neurophysiology*, **89**, 2697-2706.

Dunmyre, J.R., Del Negro, C.A. & Rubin, J.E. (2011) Interactions of persistent sodium and calcium-activated nonspecific cationic currents yield dynamically distinct bursting regimes in a model of respiratory neurons. *Journal of computational neuroscience*, **31**, 305-328.

Dutar, P., Vu, H.M. & Perkel, D.J. (1998) Multiple cell types distinguished by physiological, pharmacological, and anatomic properties in nucleus HVc of the adult zebra finch. *Journal of Neurophysiology*, **80**, 1828-1838.

Esposito, A., Demeurisse, G., Alberti, B. & Fabbro, F. (1999) Complete mutism after midbrain periaqueductal gray lesion. *Neuroreport*, **10**, 681-685.

Fee, M.S., Kozhevnikov, A. & Hahnloser, R. (2004) Neural mechanisms of vocal sequence: Generation in the songbird. *Ann. NY Acad. Sci*.

Fee, M.S. & Scharff, C. (2010) The songbird as a model for the generation and learning of complex sequential behaviors. *ILAR journal*, **51**, 362-377.

Flinker, A., Korzeniewska, A., Shestyuk, A.Y., Franaszczuk, P.J., Dronkers, N.F., Knight, R.T. & Crone, N.E. (2015) Redefining the role of Broca's area in speech. *Proceedings of the National Academy of Sciences*, **112**, 2871-2875.

Fridriksson, J., Fillmore, P., Guo, D. & Rorden, C. (2015) Chronic Broca's aphasia is caused by damage to Broca's and Wernicke's areas. *Cerebral Cortex*, **25**, 4689-4696.

Fujimoto, H., Hasegawa, T. & Watanabe, D. (2011) Neural coding of syntactic structure in learned vocalizations in the songbird. *Journal of Neuroscience*, **31**, 10023-10033.

Georgopoulos, A.P., Lurito, J.T., Petrides, M., Schwartz, A.B. & Massey, J.T. (1989) Mental rotation of the neuronal population vector. *Science*, **243**, 234-236.

Gibb, L., Gentner, T.Q. & Abarbanel, H.D. (2009a) Brain stem feedback in a computational model of birdsong sequencing. *Journal of neurophysiology*, **102**, 1763-1778.

Gibb, L., Gentner, T.Q. & Abarbanel, H.D. (2009b) Inhibition and recurrent excitation in a computational model of sparse bursting in song nucleus HVC. *Journal of neurophysiology*, **102**, 1748-1762.

Goaillard, J.-M., Taylor, A.L., Pulver, S.R. & Marder, E. (2010) Slow and persistent postinhibitory rebound acts as an intrinsic short-term memory mechanism. *Journal of Neuroscience*, **30**, 4687-4692.

Gobes, S.M. & Bolhuis, J.J. (2007) Birdsong memory: a neural dissociation between song recognition and production. *Current Biology*, **17**, 789-793.

Goldberg, J.H. & Fee, M.S. (2010) Singing-related neural activity distinguishes four classes of putative striatal neurons in the songbird basal ganglia. *Journal of neurophysiology*, **103**, 2002-2014.

Graff-Radford, N., Damasio, H., Yamada, T., Eslinger, P. & Damasio, A. (1985) Nonhaemorrhagic thalamic infarction: clinical, neuropsychological and electrophysiological findings in four anatomical groups defined by computerized tomography. *Brain*, **108**, 485-516.

Gritti, I., Manns, I.D., Mainville, L. & Jones, B.E. (2003) Parvalbumin, calbindin, or calretinin in cortically projecting and GABAergic, cholinergic, or glutamatergic basal forebrain neurons of the rat. *Journal of Comparative Neurology*, **458**, 11-31.

Gulyás, A.I., Hájos, N. & Freund, T.F. (1996) Interneurons containing calretinin are specialized to control other interneurons in the rat hippocampus. *Journal of Neuroscience*, **16**, 3397-3411.

Hahnloser, R.H., Kozhevnikov, A.A. & Fee, M.S. (2003) erratum: An ultra-sparse code underlies the generation of neural sequences in a songbird. *Nature*, **421**, 294-294.

Hahnloser, R.H., Kozhevnikov, A.A. & Fee, M.S. (2006) Sleep-related neural activity in a premotor and a basal-ganglia pathway of the songbird. *Journal of neurophysiology*, **96**, 794-812.

Halsema, K. & Bottjer, S. (1991) Lesioning afferent input to a forebrain nucleus disrupts vocal learning in zebra finches. *Neurosciences*, **17**, 1052.

Harvey, C.D., Collman, F., Dombeck, D.A. & Tank, D.W. (2009) Intracellular dynamics of hippocampal place cells during virtual navigation. *Nature*, **461**, 941-946.

Helasvuo, M.-L., Klippi, A. & Laakso, M. (2001) Grammatical structuring in Broca's and Wernicke's aphasia in Finnish. *Journal of Neurolinguistics*, **14**, 231-254.

Highnam, C.L. & Bleile, K.M. (2011) Language in the cerebellum. *American Journal of speech-language pathology*.

Hodgkin, A.L. & Huxley, A.F. (1952) A quantitative description of membrane current and its application to conduction and excitation in nerve. *The Journal of physiology*, **117**, 500-544.

Javed, K. & Lui, F. (2019) Neuroanatomy, Cerebral Cortex *StatPearls [Internet]*. StatPearls Publishing.

Javed, K. & Wroten, M. (2019) Neuroanatomy, Wernicke Area *StatPearls [Internet]*. StatPearls Publishing.

Jin, D.Z. (2009) Generating variable birdsong syllable sequences with branching chain networks in avian premotor nucleus HVC. *Physical Review E*, **80**, 051902.

Jin, D.Z., Ramazanoğlu, F.M. & Seung, H.S. (2007) Intrinsic bursting enhances the robustness of a neural network model of sequence generation by avian brain area HVC. *Journal of computational neuroscience*, **23**, 283.

Jürgens, U. (1995) Neuronal control of vocal production in non-human and human primates *Current topics in primate vocal communication*. Springer, pp. 199-206.

Katahira, K., Okanoya, K. & Okada, M. (2007) A neural network model for generating complex birdsong syntax. *Biological Cybernetics*, **97**, 441-448.

Katz, L.C. & Gurney, M.E. (1981) Auditory responses in the zebra finch's motor system for song. *Brain research*, **221**, 192-197.

Klostermann, F. (2013) Functional roles of the thalamus for language capacities. *Frontiers in systems neuroscience*, **7**, 32.

Kobayashi, K., Uno, H. & Okanoya, K. (2001) Partial lesions in the anterior forebrain pathway affect song production in adult Bengalese finches. *Neuroreport*, **12**, 353-358.

Kosche, G., Vallentin, D. & Long, M.A. (2015) Interplay of inhibition and excitation shapes a premotor neural sequence. *Journal of Neuroscience*, **35**, 1217-1227.

Kozhevnikov, A.A. & Fee, M.S. (2007) Singing-related activity of identified HVC neurons in the zebra finch. *Journal of neurophysiology*, **97**, 4271-4283.

Kubota, M. & Saito, N. (1991) Sodium‐and calcium‐dependent conductances of neurones in the zebra finch hyperstriatum ventrale pars caudale in vitro. *The Journal of physiology*, **440**, 131-142.

Kubota, M. & Taniguchi, I. (1998) Electrophysiological characteristics of classes of neuron in the HVc of the zebra finch. *Journal of Neurophysiology*, **80**, 914-923.

Lamendella, J.T. (1977) The limbic system in human communication *Studies in neurolinguistics*. Elsevier, pp. 157-222.

Leonardo, A. & Fee, M.S. (2005) Ensemble coding of vocal control in birdsong. *Journal of Neuroscience*, **25**, 652-661.

Lewicki, M.S. (1996) Intracellular characterization of song-specific neurons in the zebra finch auditory forebrain. *Journal of Neuroscience*, **16**, 5854-5863.

Lewicki, M.S. & Konishi, M. (1995) Mechanisms underlying the sensitivity of songbird forebrain neurons to temporal order. *Proceedings of the National Academy of Sciences*, **92**, 5582-5586.

Li, M. & Greenside, H. (2006) Stable propagation of a burst through a one-dimensional homogeneous excitatory chain model of songbird nucleus HVC. *Physical Review E*, **74**, 011918.

Lieberman, P. (2009) *Human language and our reptilian brain: The subcortical bases of speech, syntax, and thought*. Harvard University Press.

Long, M.A., Jin, D.Z. & Fee, M.S. (2010) Support for a synaptic chain model of neuronal sequence generation. *Nature*, **468**, 394-399.

Macklis, J.D. (1993) Transplanted neocortical neurons migrate selectively into regions of neuronal degeneration produced by chromophore-targeted laser photolysis. *Journal of Neuroscience*, **13**, 3848-3863.

Madison, R.D. & Macklis, J.D. (1993) Noninvasively induced degeneration of neocortical pyramidal neurons in vivo: selective targeting by laser activation of retrogradely transported photolytic chromophore. *Experimental neurology*, **121**, 153-159.

Marczinski, C.A. & Kertesz, A. (2006) Category and letter fluency in semantic dementia, primary progressive aphasia, and Alzheimer's disease. *Brain and language*, **97**, 258-265.

Margoliash, D. & Schmidt, M.F. (2010) Sleep, off-line processing, and vocal learning. *Brain and language*, **115**, 45-58.

Mauk, M.D. & Buonomano, D.V. (2004) The neural basis of temporal processing. *Annu. Rev. Neurosci.*, **27**, 307-340.

McConnell, S.K. (1995) Constructing the cerebral cortex: neurogenesis and fate determination. *Neuron*, **15**, 761-768.

Mehta, M., Lee, A. & Wilson, M. (2002) Role of experience and oscillations in transforming a rate code into a temporal code. *Nature*, **417**, 741-746.

Mooney, R. (2000) Different subthreshold mechanisms underlie song selectivity in identified HVc neurons of the zebra finch. *Journal of Neuroscience*, **20**, 5420-5436.

Mooney, R. (2009) Neural mechanisms for learned birdsong. *Learning & Memory*, **16**, 655-669.

Mooney, R. (2009a) Neurobiology of song learning. *Current opinion in neurobiology*, **19**, 654-660.

Mooney, R., Hoese, W. & Nowicki, S. (2001) Auditory representation of the vocal repertoire in a songbird with multiple song types. *Proceedings of the National Academy of Sciences*, **98**, 12778-12783.

Mooney, R. & Prather, J.F. (2005) The HVC microcircuit: the synaptic basis for interactions between song motor and vocal plasticity pathways. *Journal of Neuroscience*, **25**, 1952-1964.

Moorman, S., Gobes, S.M., Kuijpers, M., Kerkhofs, A., Zandbergen, M.A. & Bolhuis, J.J. (2012) Human-like brain hemispheric dominance in birdsong learning. *Proceedings of the National Academy of Sciences*, **109**, 12782-12787.

Obler, L.K., Albert, M.L., Goodglass, H. & Benson, D.F. (1978) Aphasia type and aging. *Brain and language*, **6**, 318-322.

Pastalkova, E., Itskov, V., Amarasingham, A. & Buzsáki, G. (2008) Internally generated cell assembly sequences in the rat hippocampus. *Science*, **321**, 1322-1327.

Price, C.J. (2012) A review and synthesis of the first 20 years of PET and fMRI studies of heard speech, spoken language and reading. *Neuroimage*, **62**, 816-847.

Roberts, T.F., Hisey, E., Tanaka, M., Kearney, M.G., Chattree, G., Yang, C.F., Shah, N.M. & Mooney, R. (2017) Identification of a motor-to-auditory pathway important for vocal learning. *Nature neuroscience*, **20**, 978.

Rosen, M.J. & Mooney, R. (2003) Inhibitory and excitatory mechanisms underlying auditory responses to learned vocalizations in the songbird nucleus HVC. *Neuron*, **39**, 177-194.

Satterlie, R.A. (1985) Reciprocal inhibition and postinhibitory rebound produce reverberation in a locomotor pattern generator. *Science*, **229**, 402-404.

Scharff, C., Kirn, J.R., Grossman, M., Macklis, J.D. & Nottebohm, F. (2000) Targeted neuronal death affects neuronal replacement and vocal behavior in adult songbirds. *Neuron*, **25**, 481-492.

Schmidt, M.F. & Perkel, D.J. (1998) Slow synaptic inhibition in nucleus HVc of the adult zebra finch. *Journal of Neuroscience*, **18**, 895-904.

Shea, S.D., Koch, H., Baleckaitis, D., Ramirez, J.-M. & Margoliash, D. (2010) Neuron-specific cholinergic modulation of a forebrain song control nucleus. *Journal of neurophysiology*, **103**, 733-745.

Shima, K., Isoda, M., Mushiake, H. & Tanji, J. (2007) Categorization of behavioural sequences in the prefrontal cortex. *Nature*, **445**, 315-318.

Solis, M.M. & Perkel, D.J. (2005) Rhythmic activity in a forebrain vocal control nucleus in vitro. *Journal of Neuroscience*, **25**, 2811-2822.

Stark, B.C. & Warburton, E.A. (2018) Improved language in chronic aphasia after self-delivered iPad speech therapy. *Neuropsychological rehabilitation*, **28**, 818-831.

Terman, D., Rubin, J.E., Yew, A. & Wilson, C. (2002) Activity patterns in a model for the subthalamopallidal network of the basal ganglia. *Journal of Neuroscience*, **22**, 2963-2976.

Thorpe, W.H. (1958) The learning of song patterns by birds, with especial reference to the song of the chaffinch Fringilla coelebs. *Ibis*, **100**, 535-570.

Trost, J.E. & Canter, G.J. (1974) Apraxia of speech in patients with Broca's aphasia: A study of phoneme production accuracy and error patterns. *Brain and language*, **1**, 63-79.

Troyer, T.W. & Doupe, A.J. (2000) An associational model of birdsong sensorimotor learning II. Temporal hierarchies and the learning of song sequence. *Journal of Neurophysiology*, **84**, 1224-1239.

Vu, E.T., Mazurek, M.E. & Kuo, Y.-C. (1994) Identification of a forebrain motor programming network for the learned song of zebra finches. *Journal of Neuroscience*, **14**, 6924-6934.

Wang, X.-J., Liu, Y., Sanchez-Vives, M.V. & McCormick, D.A. (2003) Adaptation and temporal decorrelation by single neurons in the primary visual cortex. *Journal of neurophysiology*, **89**, 3279-3293.

Wild, J.M., Williams, M.N., Howie, G.J. & Mooney, R. (2005) Calcium‐binding proteins define interneurons in HVC of the zebra finch (Taeniopygia guttata). *Journal of Comparative Neurology*, **483**, 76-90.